



LABORATORI NAZIONALI DI FRASCATI  
SIS – Pubblicazioni

LNF-96/002 (P)  
11 Gennaio 1996

## Physics at DAΦNE

Paula Franzini

Calçada de São Vicente, 68-2F, 1100 Lisbon, Portugal

*and*

Juliet Lee-Franzini

Laboratori Nazionali di Frascati dell'INFN

*and*

Physics department, SUNY at Stony Brook, USA.

### Abstract

A new machine at Frascati will let us observe unique interference patterns typical of quantum mechanical systems.

PACS: 11.30.Er; 13.20.Jf; 29.30.Gx; 29.40.Vj

*To be Published in Beam Line, SLAC, Stanford University, U.S.A*

## Introduction

In 1801 Young demonstrated the wave nature of light by studying the pattern obtained by shining light onto two fine slits, a pattern different from the mere superposition of the two patterns obtained from light onto each slit individually. In 1996, in Frascati, Italy, a new machine, DAΦNE, with a dedicated experiment KLOE, will measure similar interference patterns, but the physics involved will be quantum mechanical, and the particles *K mesons*, rather than photons.

## The Standard Model

Experiments involving the *K mesons* have, for some 50 years, contributed much to the construction of the present theory of elementary particles and their interactions, the *standard model*. In this model matter is made of 2 sets of particles (and their antiparticles), *quarks* (which make up the proton, e.g.), and *leptons* (the electron,  $e^-$ , for example). Forces are transmitted by another set of particles, the *gauge bosons* – the photon for the electromagnetic force, gluons for the strong force (a short range force, holding the nuclei together), and *W's* and *Z's* for the weak force (an even shorter range, weaker force, accounting, e.g., for the decay of the neutron). In the *standard model* these particles undergo strong, electromagnetic and weak *interactions*.

The quarks come in six *flavors*. In order of increasing mass, they are *u* (*up*), *d* (*down*), *s* (*strange*), *c* (*charm*), *b* (*beauty* or *bottom*), and the recently discovered *top* (*t*) quark. Only *u* and *d* quarks occur in ordinary matter, making up the proton and the neutron; the heavier quarks are short-lived, and form particles that are only seen in accelerators or cosmic rays and presumably in the very, very early universe. *K mesons*, in particular, consist of a *u* or *d* quark combined with an *s* antiquark. *B mesons*, to be studied at SLAC *en masse* in a few years, are a similar combination with *s* replaced by *b*.

## Symmetries

Particle physics also has three fundamental *symmetries*: charge conjugation (*C*), parity (*P*), and time reversal (*T*). The operation of *C* reverses the sign of all additive quantum numbers (charge, for example), but leaves momentum and spin unchanged. Fully neutral particles are transformed into themselves under this operation, and, depending on their nature, may have a positive or negative *charge conjugation quantum number*. Electromagnetic and strong interactions conserve this quantum number, while the weak interaction does not.

Parity  $P$  is the symmetry relating a physical system and its mirror image; thus a particle with left-handed helicity turns into one with right-handed helicity. Parity, like charge conjugation, is violated only in weak interactions. The neutrino,  $\nu$ , (the elusive neutral partner of the electron) is an illustration of both  $C$  and  $P$  violation, since only left-handed neutrinos and right-handed antineutrinos seem to exist ( $C$  applied to a left-handed neutrino would produce a left-handed antineutrino, while  $P$  would produce a right-handed neutrino, both of which are not observed). It was a shock when  $C$  and  $P$  violation were predicted in weak interactions in 1956 and discovered in 1957. These violations are not subtle; they can be 100%.

For some years after the discovery of  $C$  and  $P$  violation, it was thought that the combined symmetry  $CP$  might still be valid. Under  $CP$ , a left-handed neutrino turns into a right-handed antineutrino. Indeed,  $CP$  is a valid symmetry of almost all interactions: the *one* exception is an *observed* minute violation of one part in a thousand in the  $K$ -meson system, discovered in 1964 as explained in the next section and again greeted with great surprise. The origin of this violation is one of the outstanding puzzles of particle physics today, and its exploration is the main *raison d'être* of DAΦNE. Aside from being intellectually a great challenge, one notes that the existence of  $CP$  violation provides the only means by which we could query the inhabitants of a distant part of the universe and determine whether their world consists predominantly of matter or *antimatter* (assuming we transfer information in photons, without exchanging any matter) – the sign of the parameter measuring  $CP$  violation will be opposite in an ‘antiuniverse,’ while all other observables will be the same. Thus  $CP$  violation also holds the key to the composition of our universe, in particular, the apparent absence of matter in it.

The third symmetry, time reversal  $T$ , relates a physical process with its equivalent ‘run backwards’ in time. This symmetry is valid for all interactions, except, as we explain below, an *inferred* minute violation in the  $K$  system. The three-fold combination  $CPT$  is a very important symmetry. It is valid, regardless if any one, or two combined symmetries are violated, for any physical process described by *quantum field theory*, the fundamental fabric of all particle physics theories as we know them. It is thus that violation of  $CP$  in the  $K$  system implies  $T$  violation. This symmetry predicts that particles and their antiparticles should have the same mass and lifetimes. It is in the  $K$ -meson system that this test can be carried out to its ultimate accuracy (see section on interference).

## The $K$ System

While of course evidence for  $CP$  violation in a new system, thus for example at the SLAC  $B$ -factory, is eagerly awaited,  $CP$  violation's cradle and so far only haunt is the neutral  $K$  system.

For the strong and electromagnetic interactions, the  $K^0$  (a  $d$  plus a  $\bar{s}$ ) and the  $\bar{K}^0$  ( $\bar{d}s$ ) are distinct particles, protected by the  $C$  symmetry from changing into each other. The weak interaction, however, violating  $C$ , allows both these particles to decay to, e.g., two  $\pi$  mesons (a combination of 2  $u$  or  $d$  quarks and their antiquarks), and therefore, at second-order, to change into each other. Thus, we speak of  $K^0$  and  $\bar{K}^0$  as distinct particles because they are *produced* by the strong interaction, but when it comes to their decay, by the weak interaction, it no longer makes sense to speak of them as distinct.

If  $CP$  were a perfect symmetry, the physical particles would be the symmetric and antisymmetric combinations of  $K^0$  and  $\bar{K}^0$ . These, called  $K_1$  and  $K_2$ , are respectively even and odd under  $CP$ , and as a result must decay respectively to two and three pions. Since the mass of 3 pions is very close to the  $K$  mass, there is a lack of what is called *phase space*, and the  $K_2$  is thus much longer lived.  $K^0$  mesons of two very different lifetimes were observed 1956; in 1964, the observation that the  $K_0$  with a long lifetime decays a minute fraction of the time to two pions, proved unambiguously that  $CP$  also is violated. Instead of  $K_1$  and  $K_2$ , the physical states are now  $K_S$  and  $K_L$ , where  $K_S$  is  $K_1$  with a small admixture of  $K_2$ , and  $K_L$  is  $K_2$  with a small admixture of  $K_1$ . The amount of this admixture is parametrized by the  $CP$  violation parameter  $\epsilon$ , which has the measured value  $|\epsilon| = (2.259 \pm 0.018) \times 10^{-3}$ .

The story of  $CP$  violation has a final twist. In addition to the well-measured  $CP$  violation just described, coming from the admixture of  $K_1$  in  $K_L$ , there is the possibility of *direct*  $CP$  violation, in the decay of  $K_2$ . Physically, it turns out that this can be measured in the difference in the  $CP$  violation in the neutral and charged  $\pi$  decays of the  $K$ 's. This *direct*  $CP$  violation is parametrized by the quantity  $\epsilon'$ . Thirty years of measurements of  $\epsilon'$  have not been able to determine if  $\epsilon'$  is zero or not, but have found that it is much smaller than even  $\epsilon$ . Increasingly accurate measurements have only chased it closer and closer to zero. Currently it is known to be between zero and three thousandths of  $\epsilon$ . DAΦNE is being built to reduce the uncertainty by another factor of ten. This precision measurement of  $\epsilon'$  would give us an important clue as to whether the *standard model* which predicts its

value to be on the order of a few  $\times 10^{-4}$ , despite of its phenomenal success, is sufficient, or whether it does require modifications.

### DAΦNE

To reach the desired accuracy in  $\epsilon'$  requires the observation of some five million  $K_L \rightarrow 2\pi$  decays among five billion  $K_L$  decays. One way to obtain these astronomical numbers of  $K_L$  is to build a *particle factory* which produces a single, known particle of approximately twice the K-mesons mass,  $\phi$ . The  $\phi$  is the lightest vector meson composed of a strange quark and an anti-strange quark, therefore the lightest copiously producible particle decaying to two kaons. In June 1990 the first *particle factory* project, DAΦNE, was funded by the Istituto Nazionale di Fisica Nucleare, INFN, of Italy, and was christened DAΦNE, for Double Anular  $\Phi$ -factory for Nice Experiments. DAΦNE is an  $e^+e^-$  collider, where electrons and positrons of 510 million electron volts (MeV) are hurled at each other head on. At this total energy of 1019.4 MeV, the cross section (the effective target area displayed by the electrons and positrons to each other) for producing a  $\phi$  is very large, approximately  $5 \times 10^{30} \text{ cm}^{-2}$ , with negligible accompanying background. DAΦNE's target luminosity, a measure of the collision frequency per unit cross section, is  $\mathcal{L} = 10^{33} \text{ cm}^{-2}\text{s}^{-1}$ , which means 5000  $\phi$ 's are produced per second. Using the canonical high energy physics definition of one 'physics year' = ten million seconds (one third of an actual year, to account for down time, maintenance, fine tuning etc.), this means fifty billion  $\phi$ 's per year!

The  $\phi$  decays into charged kaon pairs about half of the time. These kaons move at a quarter of the speed of light ( $c$ ), and on average travel about 1 meter before they in their turn decay. In 1 'physics' year, 25 billion pairs are produced. Another third of the time, the  $\phi$  decays into a pair of neutral kaons, moving at  $\frac{1}{5}c$ . Moreover, the kaons produced at DAΦNE are not just any kaons, but kaons in a well-defined quantum-mechanical and kinematic state: one of them is always a  $K_S$ , at DAΦNE travelling on average 6mm. The other kaon is always a  $K_L$ , travelling on average 3.5 m. In a 'physics' year, 15 billion  $K_S K_L$  pairs are produced.

Fig. 1 is a schematic drawing of DAΦNE. There are two interaction areas, for the two experiments KLOE (particle physics) and FINUDA (nuclear physics), and also the possibility for lower energy research and medical research with the ultraviolet and x-ray beams of the DAΦNE-L(ight) facility. The DAΦNE main rings are 98 meters in perimeter, in a roughly rectangular shape, of 32 by 23 meters. When DAΦNE turns on, at one tenth

of its final luminosity, it will already have about the same number of particles in its 98 m ring as LEP currently has in its 27 km ring.

### The How of DAΦNE

What makes a factory? The luminosity of a collider is given by  $\mathcal{L} = fnN_1N_2/A$ . Here  $n$  is the number of bunches (rather than being uniformly distributed, the particles in DAΦNE are gathered into several (30-120) flat (3 cm long by 3 mm wide by 0.02 mm high) *bunches*, spaced at roughly one meter intervals);  $f$  the revolution frequency (how many times around the collider the bunches go per second);  $N_i$  the number of particles per bunch for each species of particle, and  $A$  the area of the beams (for fully overlapping beams). Thus, many bunches of many particles, going around at a high frequency, focussed tightly into beams of a very small area, produce a high luminosity. Nonetheless, whichever of these parameters are modified to produce a larger luminosity, without radically new technology, the luminosity in a single ring machine will be limited by what is known as *beam-beam interactions* to be about that of current machines. The beams get 'shook up' and thus the small bunch size needed for high luminosity gets destroyed; bunches containing more particles lead to stronger shaking. Multiple bunches in a single ring do not help; each bunch 'sees' all of its counterparts and gets successively more and more perturbed.

The solution generally found in 'factories' is to have two separate rings (hence the DA in DAΦNE, for Double Anular), which cross each other at a small but non-zero *crossing angle* (about 1 degree for DAΦNE). This crossing angle is needed, even though head-on collisions are less disruptive to the beam, because if the two beams were parallel even for a few meters, each bunch would then pass several of its counterparts in a small machine like DAΦNE, where there will eventually be more than one bunch per meter.

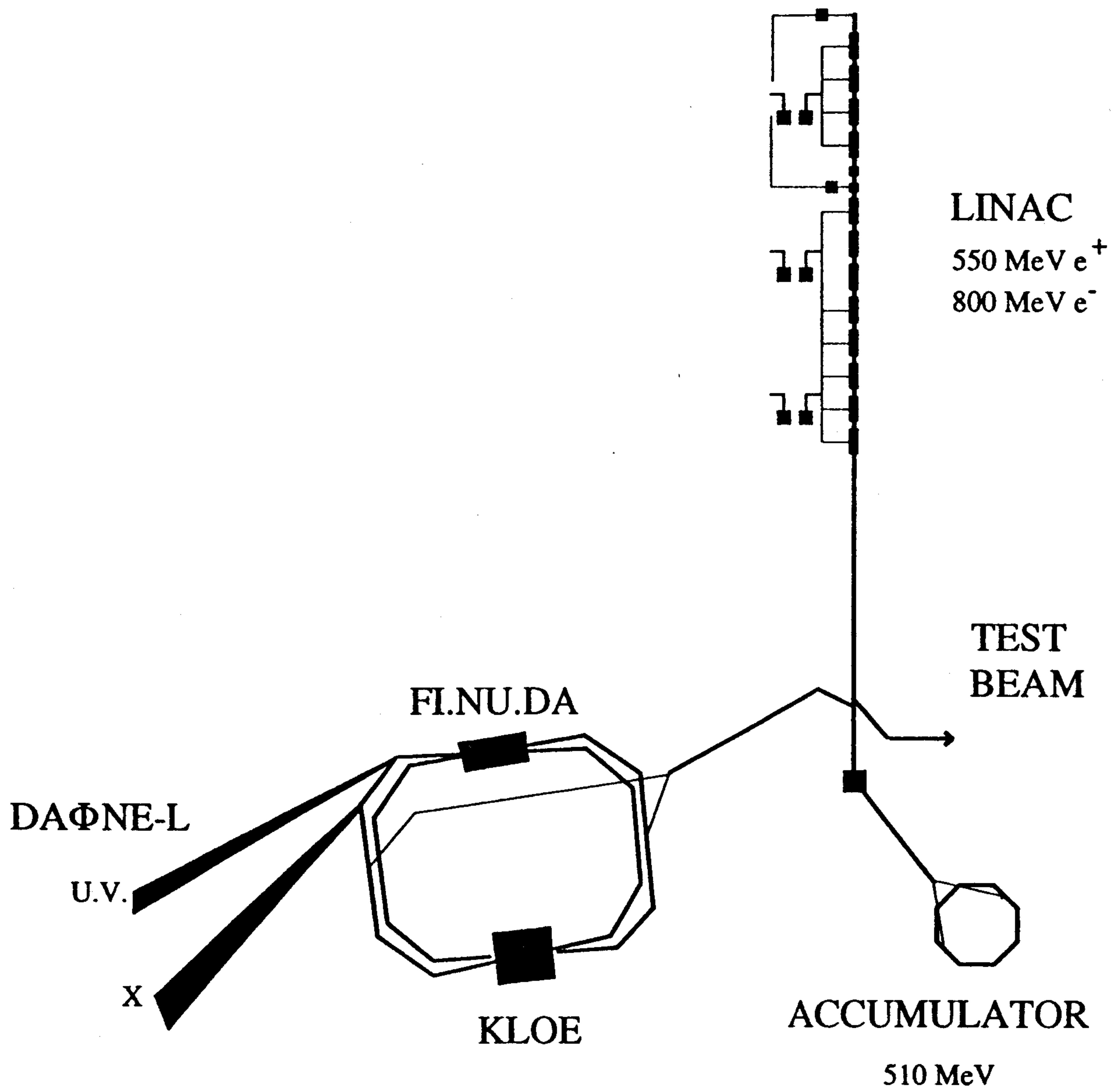


Fig. 1. The DAΦNE machine complex.

### Interference at DAΦNE

At DAΦNE neutral  $K$ -meson pairs from  $\phi$  decays are produced in a pure  $C$ -odd quantum state. It turns out that this means the observation of a  $K_S$  ( $K_L$ ) signals, and indeed guarantees, the presence of a  $K_L$  ( $K_S$ ) of opposite momentum; in other words we will *never* have a decay with two  $K_S$  or two  $K_L$ . This gives DAΦNE unique advantages for the study of  $CP$  and  $CPT$  violation: because of the quantum mechanical coherence of the initial two kaons state, interference phenomena can be observed without identification of  $K_S$ 's or  $K_L$ 's. One can understand this by analogy with the classical experiment of shining a light onto two slits and observing the spatial pattern on a screen beyond, without knowing from which slit the photons came. One notes that the pattern observed when both holes are open is not the mere superposition of that obtained when one hole alone is open added to when the other hole alone is open, because of the phase relationship between the waves, and one gets a complex pattern. In a similar way, at DAΦNE, the intensity distribution one observes depends on which final states are involved, as described below. In short, one can perform a whole spectrum of precision “ $K$ -meson interferometry” experiments at DAΦNE by measuring the decay intensity distributions of the  $K$ -meson pair as a function of the distance between the two decay vertices for appropriate choices of the two final states.

If we label the final state of one  $K$  by  $f_1$ , and the time at which the decay occurs by  $t_1$ , and similarly  $f_2$  and  $t_2$  for the other  $K$ , by varying the time difference  $t_1 - t_2$  and the final states examined, it is possible to measure many different parameters describing  $CP$  and  $CPT$  violation. The interference term is sensitive to the mass difference between  $K_S$  and  $K_L$ . For example,

1. with  $f_1 = \pi^+\pi^-$ ,  $f_2 = \pi^0\pi^0$ , as illustrated in Fig. 2a, one measures the real part of  $\epsilon'$  at large time differences, and the imaginary part of  $\epsilon'$  at short time differences. Fig. 2b shows destructive interference pattern for this case.



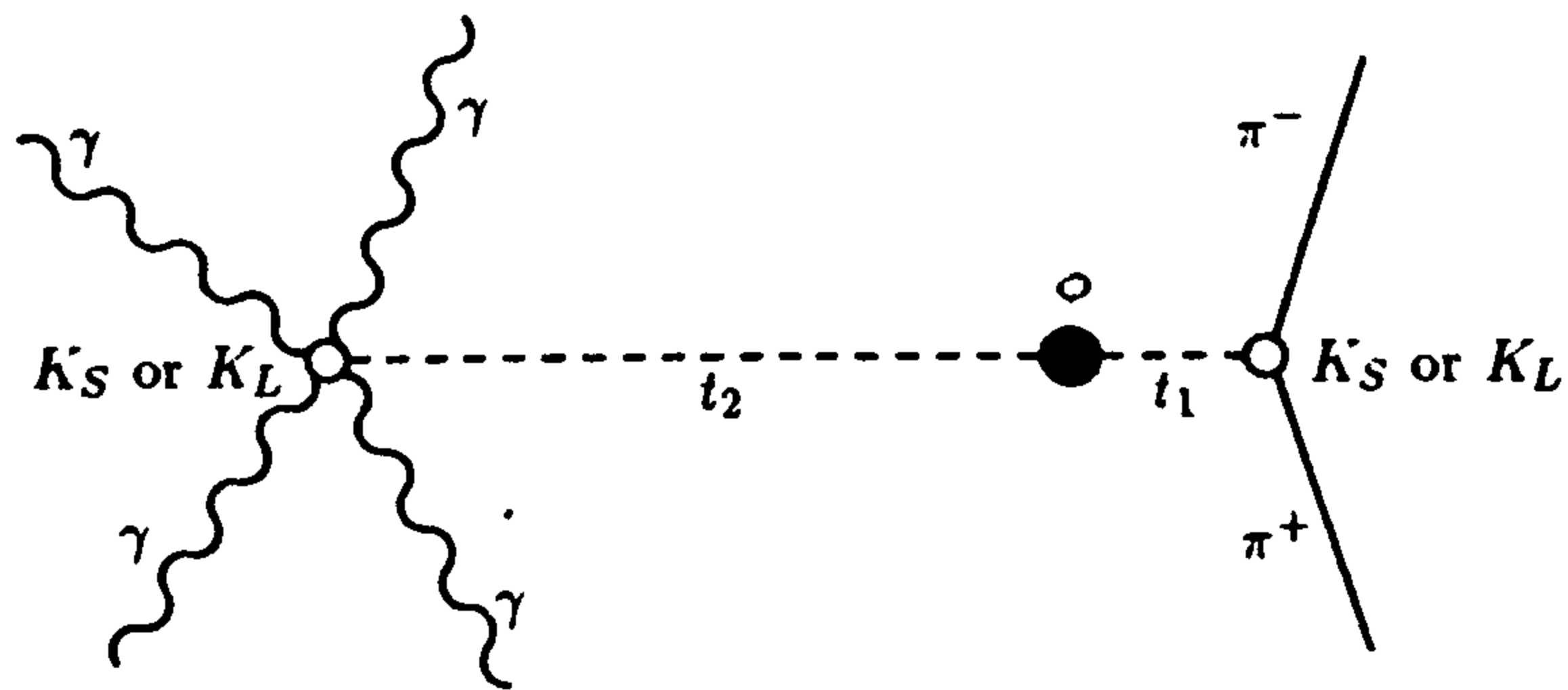


Fig. 2a. A  $\phi$  (the black dot) decaying to two  $K$ 's (the white dots) in turn decaying at times  $t_1$  and  $t_2$  to the final states  $f_1 = \pi^+ \pi^-$  and  $f_2 = \pi^0 \pi^0$  (each  $\pi^0$  decays finally to two photons).

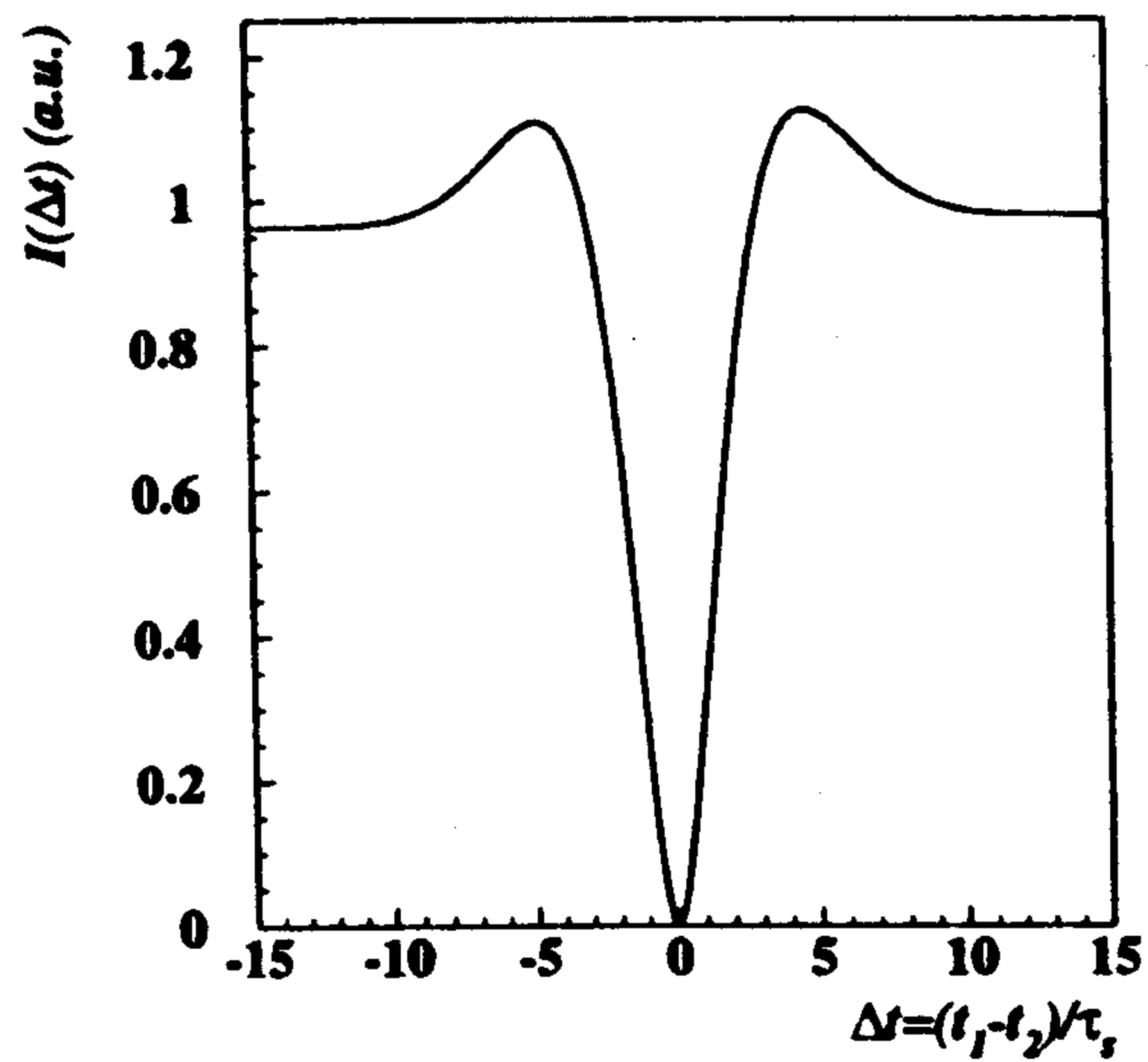
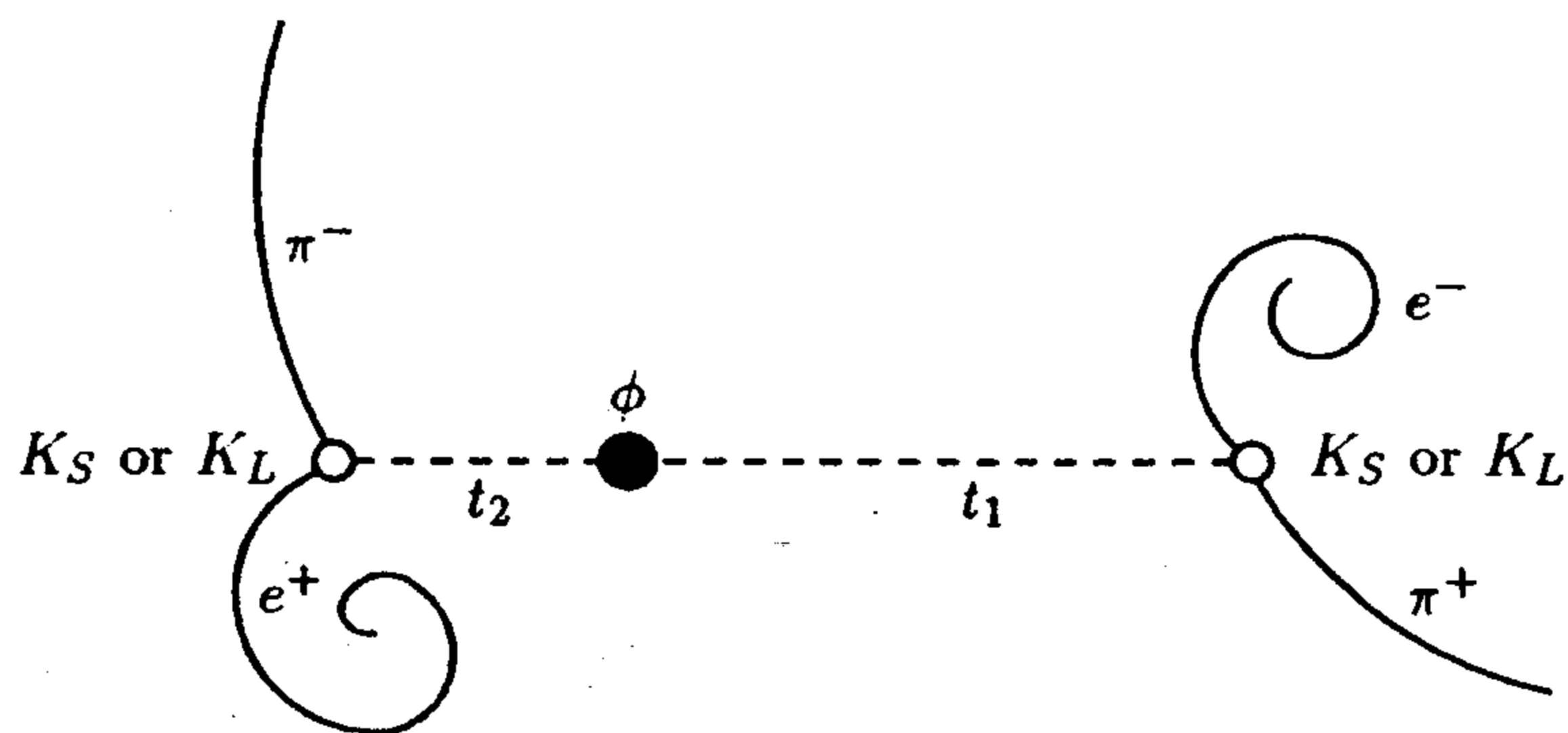


Fig. 2b. Interference pattern for  $f_1 = \pi^+ \pi^-$ ,  $f_2 = \pi^0 \pi^0$ .

2. With  $f_1 = \pi^+ e^- \bar{\nu}$  and  $f_2 = \pi^- e^+ \nu$ , as illustrated in Fig. 3a, one can measure the  $CPT$ -violation parameter, in other words, test whether  $CPT$  is violated, and in fact weigh the relative masses of the  $K^0$  and  $\bar{K}^0$ , to one part in a quintillion ( $10^{18}$ )! Fig. 3b shows the constructive interference pattern, in this case.

Many other patterns result from choosing different decay channels; from them we can learn all about the neutral  $K$ -meson system, that is, determine the total set of 16 parameters which define the system. No other experiment at any other high energy accelerator can do this.



**Fig. 3a.** A  $\phi$  (the black dot) decaying to two  $K$ 's (the white dots) in turn decaying at times  $t_1$  and  $t_2$  to the final states  $f_1 = \pi^+ e^- \bar{\nu}$ ,  $f_2 = \pi^- e^+ \nu$ . Note that the neutrinos are not depicted because they are 'invisible' particles.

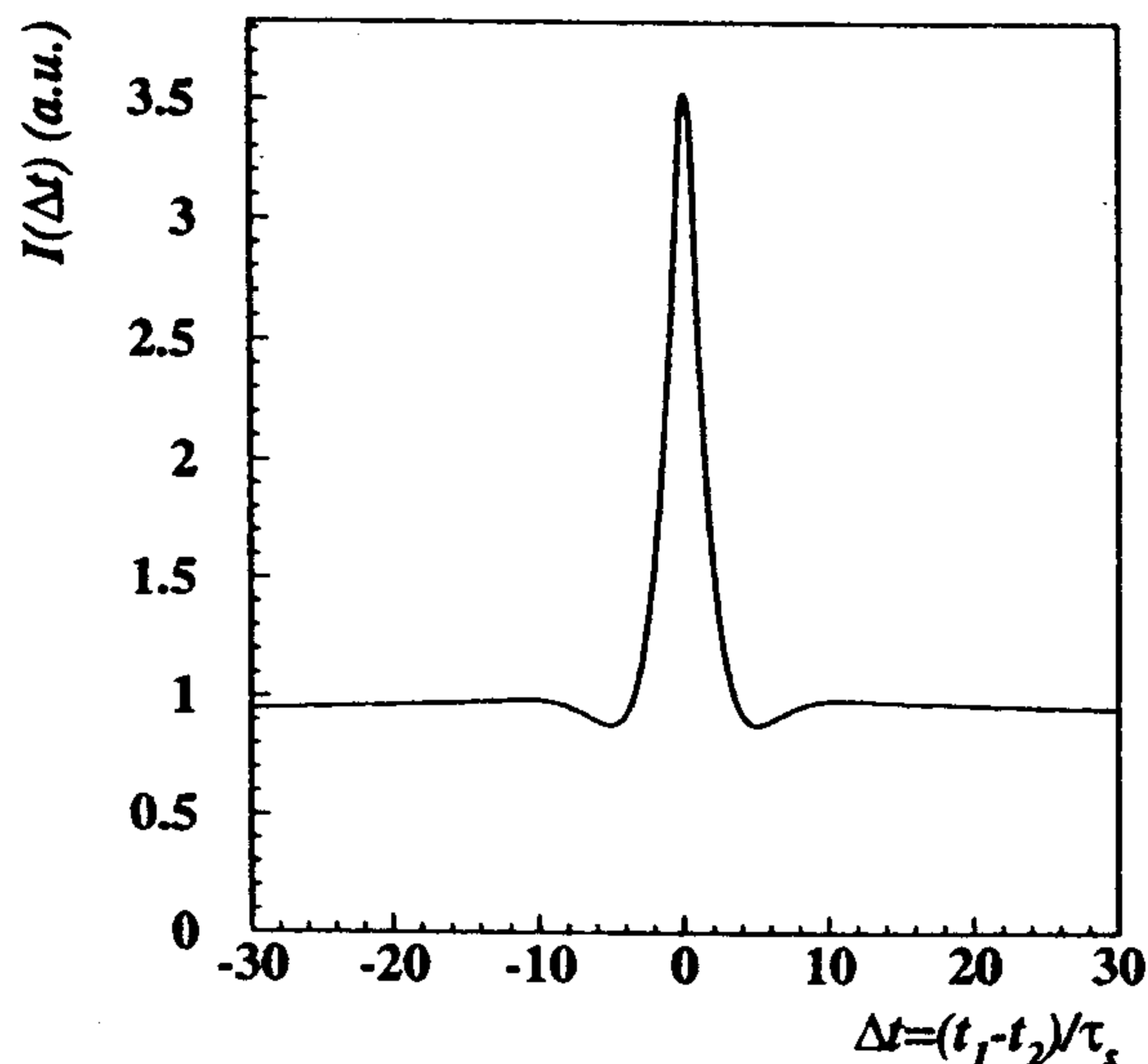


**Fig. 3b.** Interference pattern for  $f_1 = \pi^+ e^- \bar{\nu}$ ,  $f_2 = \pi^- e^+ \nu$ .

## KLOE

The KLOE detector's main mission is to study  $\epsilon'$  with a sensitivity of the order of one part in ten thousand via traditional branching ratio methods as well as through a whole host of *quantum interferometry* measurements. It is also fully capable of investigating a whole range of other physics. The scale of KLOE is driven by a fundamental parameter, the average distance the  $K_L$  goes before decaying (3.5 m). A practical compromise is to detect  $K_L$  decays in a big, cylindrical chamber of radius  $\sim 2$  m and length 370 cm. The KLOE cross section is shown in fig. 4.

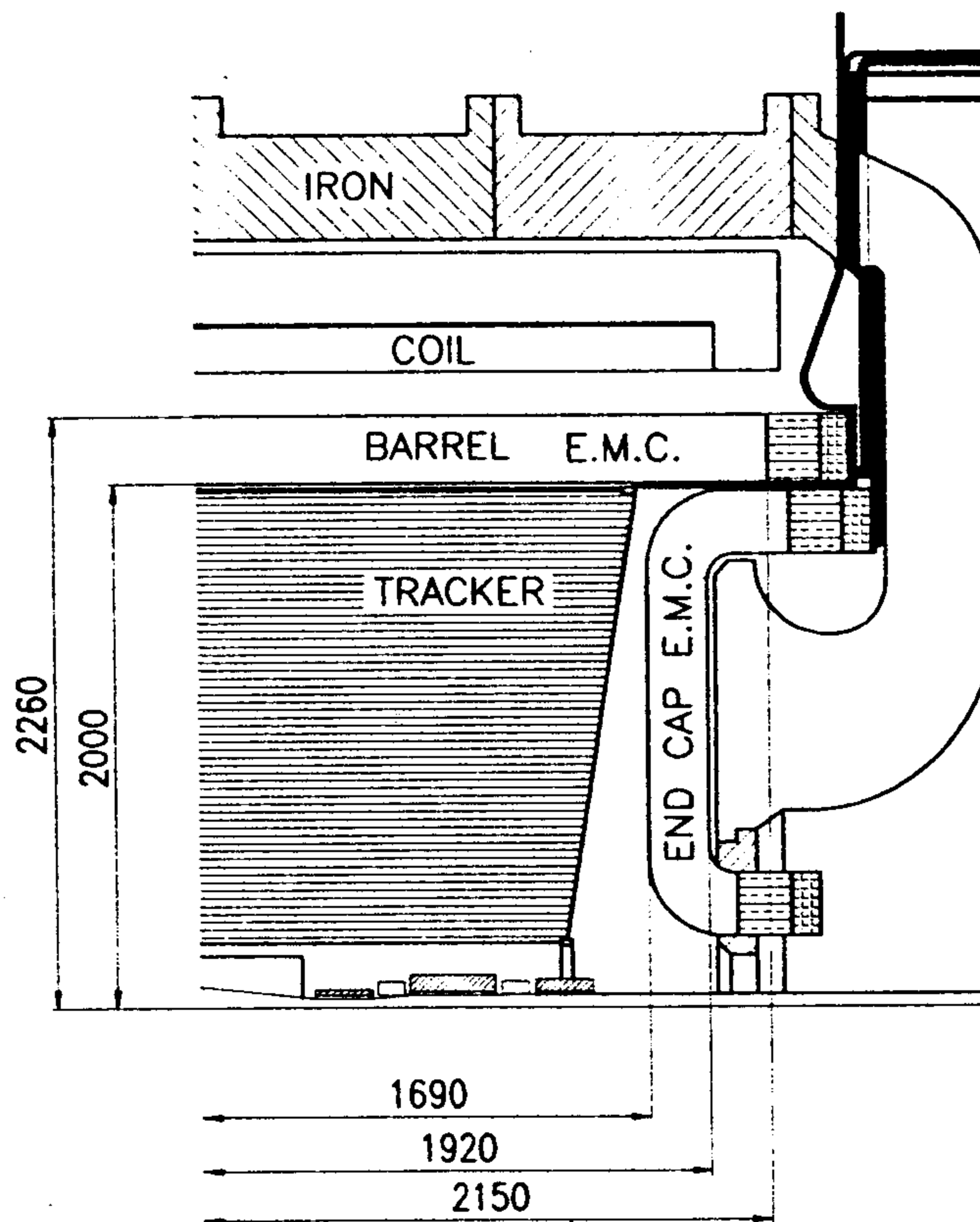


Fig. 4. KLOE cross section along the beam axis.

Detector requirements are to: 1) collect enough statistics, 2) measure the path length of the  $K_S$ ,  $K_L$  decays to the required accuracy, 3) reject backgrounds at the desired level, and 4) be self-calibrating. Thus, the experimental apparatus must be able to track charged particles of momenta between 50 and 250 MeV/c. It must also detect with very high efficiency (i.e., low failure rate) photons with energy as low as 20 MeV, measure their energies with a fractional resolution of 15% at 100 MeV, and provide the space coordinates of the photon conversion point, where the daughter photons from a  $\pi^0$  became

an electron-positron pair. A largely empty space, with a special gas and fifty thousand fine wires, lets us see where the charged particles went. The photon measurements are done in a lead-scintillating fiber sampling electromagnetic calorimeter (EmC), with exceptional timing abilities, which surrounds the tracking chamber. It is in turn surrounded by a superconducting coil providing a solenoidal field of 0.6 T.

### The How of KLOE

The radius of the beam pipe around the luminous point is 10 cm. This allows the definition of a clean fiducial region for  $K_S$  decays. The beam pipe is made of 0.5 mm thick beryllium to minimize multiple scattering, energy loss for charged kaons and  $K_L \rightarrow K_S$  regeneration.

The almost uniform distribution of  $K_L$  decay vertices and secondary tracks in the chamber volume requires a constant size drift cell. This is achieved by using only alternating stereo layers, with constant inward radial displacement at the chamber center. The total number of cells is  $\sim 12,000$ . We use helium-based gas mixtures, aluminum wires, as well as spherically shaped carbon fiber endwalls to minimize materials seen by the photons entering the electromagnetic calorimeter.

Unique to the KLOE experiment, is the method of determining the flight path of  $K_L$ , the segment ID in fig. 5, by time measurements. I is the  $\phi$  decay point, the direction of ID is given by  $-\mathbf{p}_{K_S}$ , and A is the photon conversion apex in the calorimeter. As illustrated in fig. 5, the flight time measurements for even a single photon of the four from  $\pi^0\pi^0$  allow the determination of the  $K_L$  decay path. The time of arrival of a photon gives the flight path of the  $K^0$  to an accuracy  $\delta l = \beta_{K_S} c \delta t \sim 6 \times 10^{-3} \text{ cm} \times \delta t(\text{ps})$ . For a 510 MeV  $K^0$ , one expects a time resolution of  $\sim 100$  ps and a path resolution of 0.6 cm.

The KLOE EmC is a hermetic, very fine sampling lead scintillating fiber calorimeter, with photomultipliers (PMs) read-out. The energy resolution is given by  $\sigma_E/E \sim 5\%/\sqrt{E(\text{GeV})}$  and the time resolution by  $\sigma_T \sim 60\text{ps}/\sqrt{E(\text{GeV})}$ .

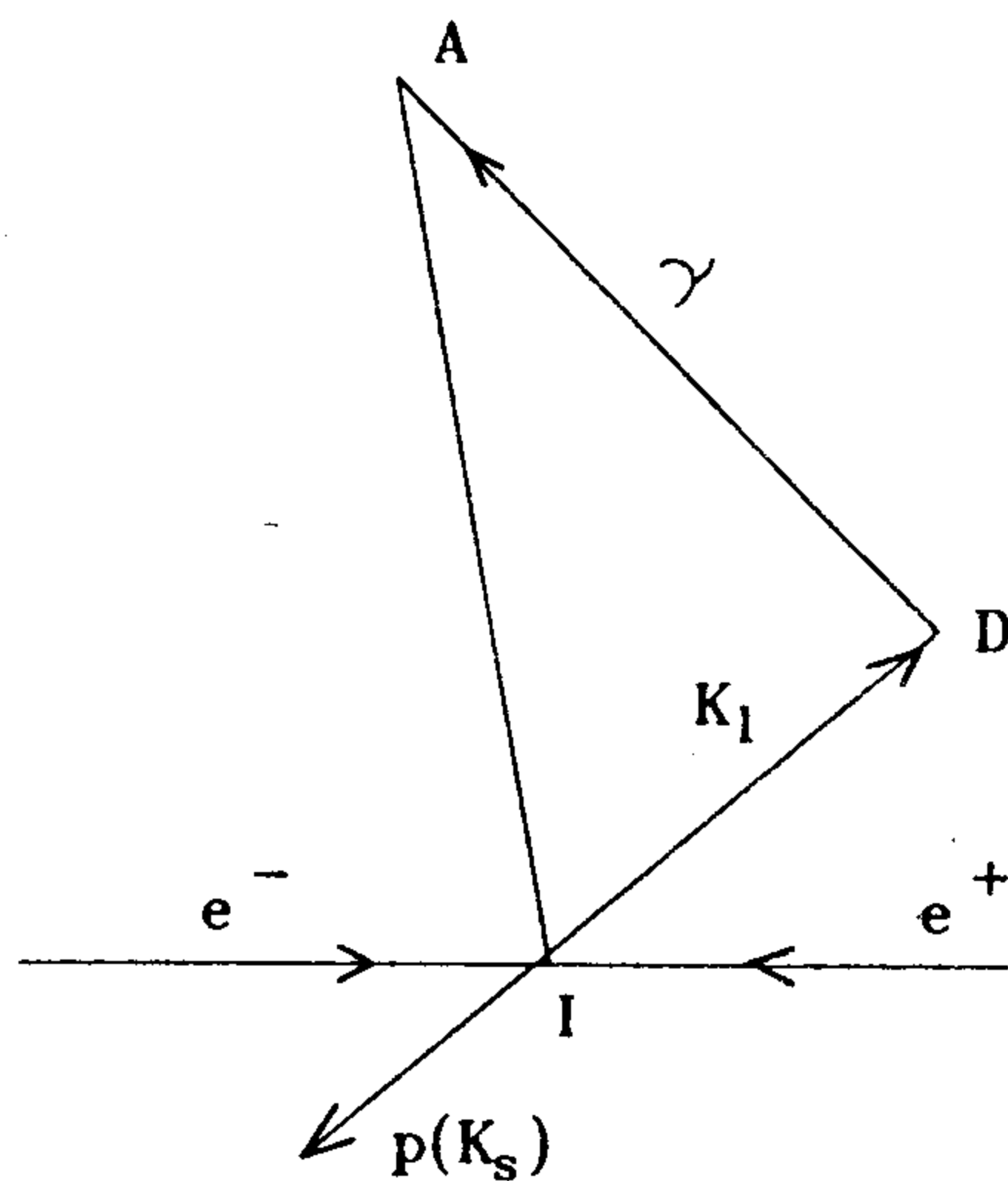


Fig. 5. Measuring the  $K_L$  decay length.

### Conclusion

Since DAΦNE is a prolific source of charged  $K$ -mesons, not only can  $CP$  studies be pursued in that system as well, one can also further the knowledge of the low energy meson theory known as *chiral perturbation theory*. It also is a perfect laboratory for light meson spectroscopy and nuclear physics. Still, for the KLOE experimenters the thrill is really the opportunity to perform the most accurate tests and measurements in particle physics while being able to actually observe beautiful interference patterns in a quantum mechanical system.

**References** All references are included in the Appendix, which is a write up of lectures given by Juliet Lee-Franzini at the **5th Hellenic School and Workshops on Elementary Particle Physics** in Corfu, 3-24 September 1995.

### Appendix

#### Physics at DAΦNE with KLOE

PHYSICS AT DAΦNE WITH KLOE

Juliet Lee-Franzini  
 Laboratori Nazionali di Frascati  
 Via Enrico Fermi 40 - 00044 - Frascati, Italy  
 Physics Department, State University of New York at Stony Brook  
 Stony Brook, New York 11794, U.S.A.

ABSTRACT

A general purpose detector, KLOE, is being constructed for use at DAΦNE, the  $\phi$ -factory at LNF, Frascati. While it is designed primarily for  $CP$  violation measurements and other symmetry studies, it is also capable of doing a whole spectrum of other experiments, from tests of chiral perturbation predictions to detailed light meson spectroscopy.

1 – KLOE'S Physics Program

1. 1  $CP$  and  $CPT$  by quantum interferometry

Consider the process  $\phi \rightarrow K\bar{K} \rightarrow f_1, t_1 + f_2, t_2$  where a  $K^0$  meson decays into a state  $f_1$  at time  $t_1$  and the other into a state  $f_2$  at time  $t_2$ , as illustrated below.



The decay intensity to  $f_1, f_2$ , as a function of  $\Delta t = t_1 - t_2$  and for  $\Delta t > 0$ , is:

$$I(f_1, f_2; \Delta t) = \frac{1}{2\Gamma} |\langle f_1 | K_S \rangle \langle f_2 | K_S \rangle|^2 \left( |\eta_1|^2 e^{-\Gamma_L \Delta t} + |\eta_2|^2 e^{-\Gamma_S \Delta t} - 2|\eta_1||\eta_2| e^{-\Gamma \Delta t / 2} \cos(\Delta m \Delta t + \phi_1 - \phi_2) \right)$$

where  $\eta_i = \langle f_i | K_L \rangle / \langle f_i | K_S \rangle$  and a similar expression holds for  $\Delta t < 0$ . The interference term is sensitive to  $\Delta m$ , the magnitudes of the amplitude ratios  $\eta$ 's and their phase difference, while the complete distribution depends also on the  $K_S$  and  $K_L$  lifetimes. One can thus perform a whole spectrum of precision "kaon-interferometry" experiments at DAΦNE by measuring the above decay intensity distributions for appropriate choices of the final states  $f_1, f_2$ . Four examples are listed below.

1. With  $f_1 = f_2$  one measures  $\Gamma_S, \Gamma_L$  and  $\Delta m$ , since all phases cancel. Rates can be measured to  $\times 10$  improvement in accuracy and  $\Delta m$  to  $\times 2$ .
2. With  $f_1 = \pi^+ \pi^-, f_2 = \pi^0 \pi^0$ , one measures  $\Re(\epsilon'/\epsilon)$  at large time differences, and  $\Im(\epsilon'/\epsilon)$  for  $|\Delta t| \leq 5\tau_s$ . Fig. 6 shows the interference pattern for this case.
3. With  $f_1 = \pi^+ \ell^- \nu$  and  $f_2 = \pi^- \ell^+ \nu$ , one can measure the  $CPT$ -violation parameter  $\delta_K$ :<sup>[1]</sup> its real part at large time differences and the imaginary part for  $|\Delta t| \leq 10\tau_s$ . Fig. 7 shows the interference pattern.
4. For  $f_1 = 2\pi, f_2 = \pi^+ \ell^- \nu$  or  $\pi^- \ell^+ \nu$  small time differences yield  $\Delta m, |\eta_{\pi\pi}|$  and  $\phi_{\pi\pi}$ , while at large time differences, the asymmetry in  $K_L$  semileptonic decays provides tests of  $T$  and  $CPT$ . The vacuum regeneration interference is shown in fig. 8.

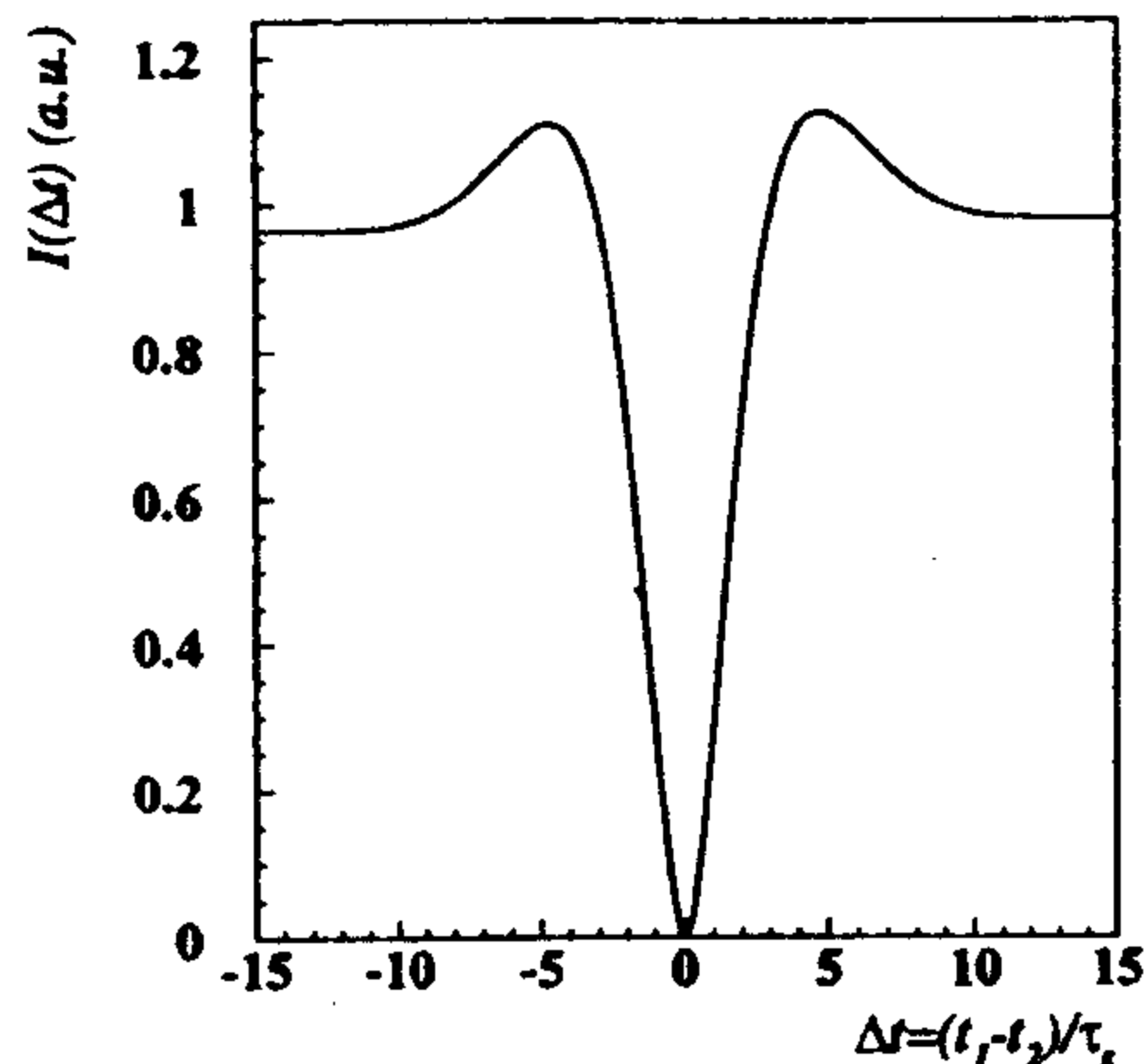


Fig. 6. Interference for  $f_1 = \pi^+ \pi^-$ ,  $f_2 = \pi^0 \pi^0$ .

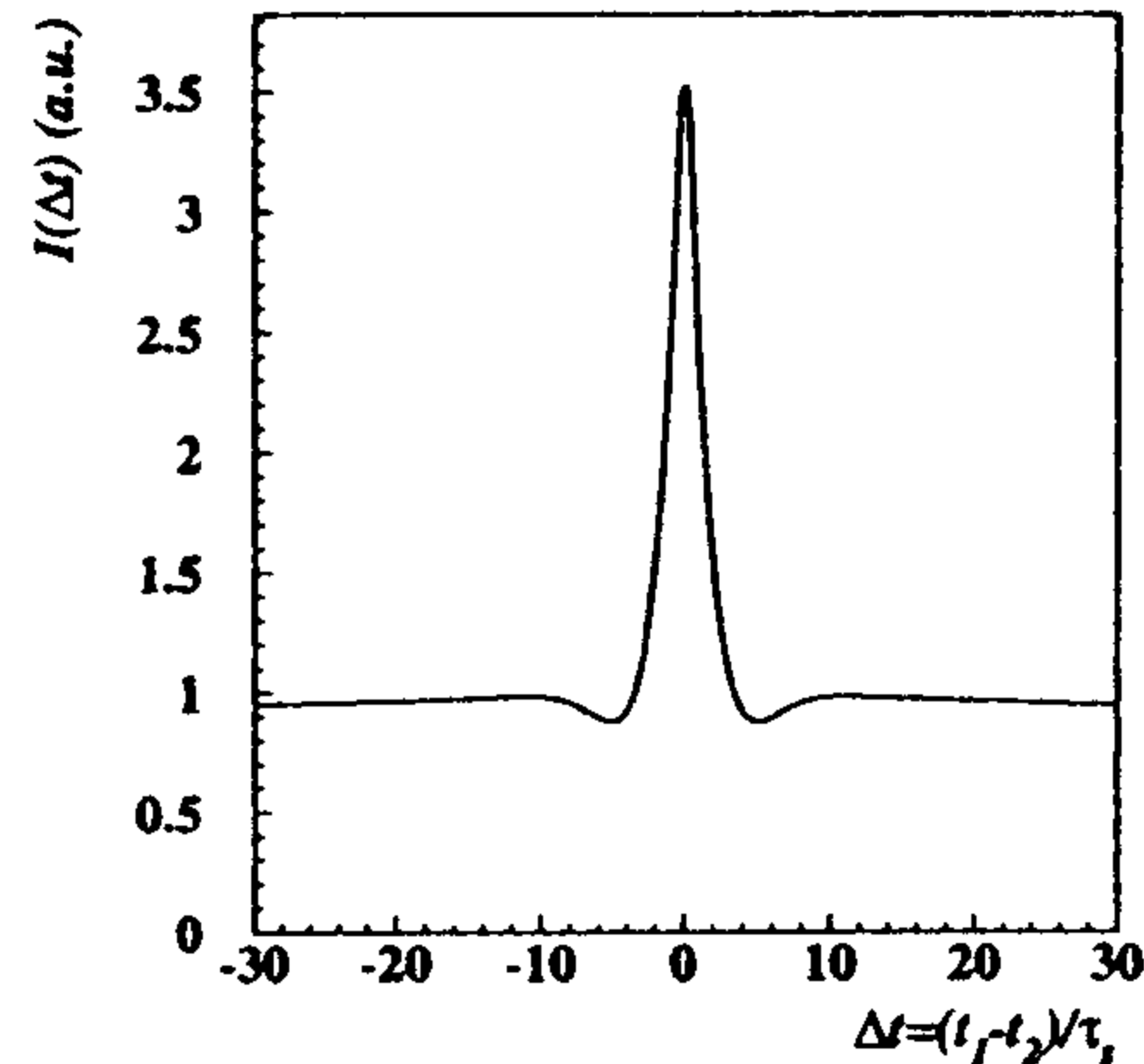


Fig. 7. Interference for  $f_1 = \ell^-$ ,  $f_2 = \ell^+$ .

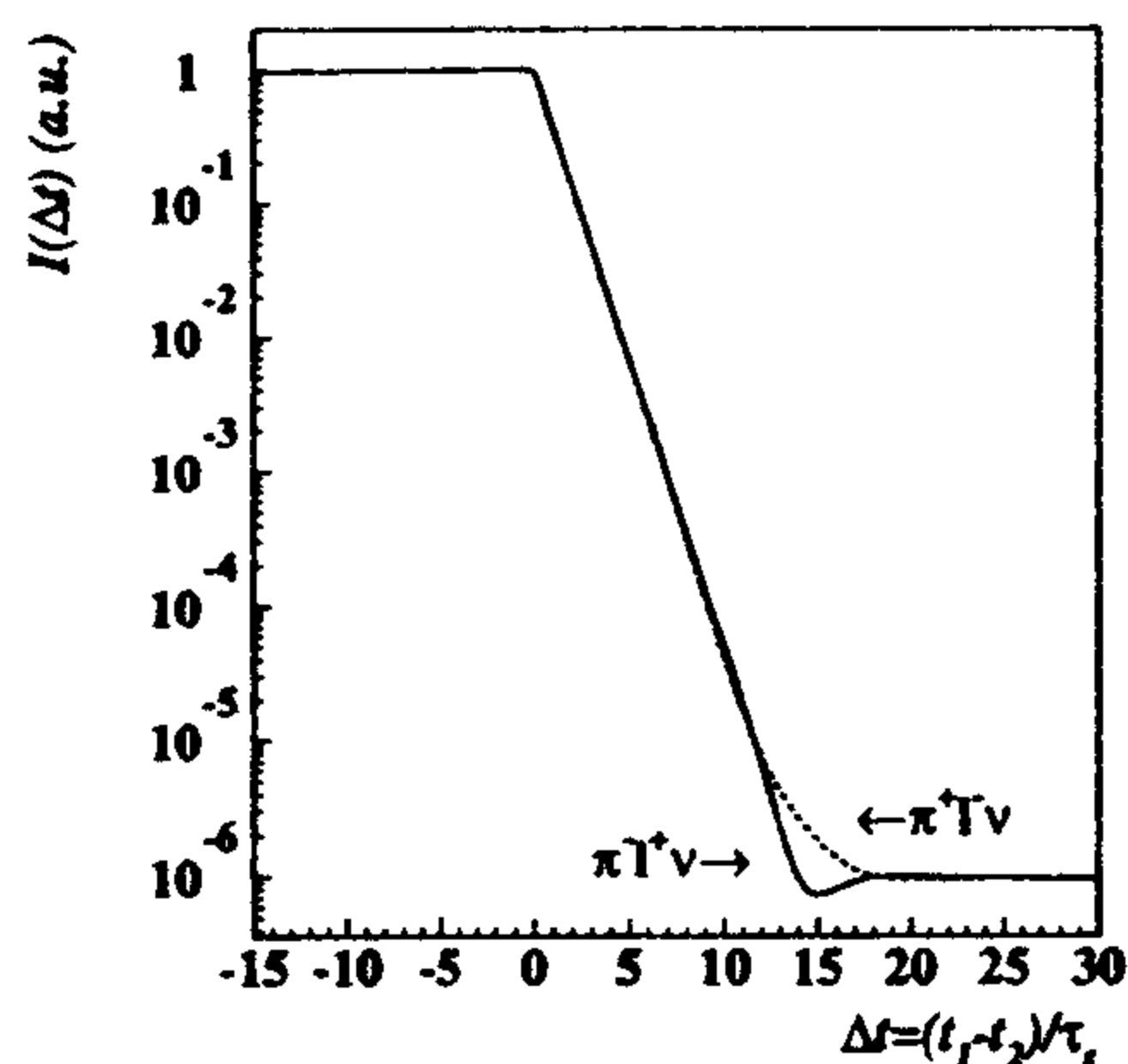


Fig. 8. Interference pattern for  $f_1 = 2\pi$ ,  $f_2 = \ell^\pm$ .

In all, by choosing appropriate  $f_1$  and  $f_2$  channels one can determine 16 independent parameters describing the neutral  $K$  system. If the validity of the  $\Delta S = \Delta Q$  rule is assumed there are only 13 parameters to be determined. Experiments at DAΦNE can thus test  $CPT$  invariance, in addition to studying  $CP$  violation. Should however the  $\Delta S = \Delta Q$  rule not hold (it is expected to be violated to only one part in  $10^7$  in the Standard Model), there are in fact 17 independent parameters.<sup>[2]</sup> Therefore we will need to use strangeness tagged  $K^0$ 's, which can be obtained from charge exchange of  $K^+$  mesons, in turn tagged by observation of a  $K^-$  meson from the copious decay  $\phi \rightarrow K^\pm$ .

### 1. 2 Measuring $\mathcal{R}^\pm/\mathcal{R}^0$

We can also use the classical method of the double ratio  $\mathcal{R}^\pm/\mathcal{R}^0 = 1 + 6 \times \Re(\epsilon'/\epsilon)$ , and other ways of measuring  $\Re(\epsilon'/\epsilon)$  from selected final states. Very different systematics are involved, thus allowing a self-check of the results. In fact, one can illustrate the statistical accuracy achievable at DAΦNE easily using the double ratio method (recall that the tagging efficiency drops out identically here and thus do not contribute to systematic errors).

In abbreviated form, the double ratio is

$$\mathcal{R}^\pm/\mathcal{R}^0 = \frac{N_L^\pm/N_S^\pm}{N_L^0/N_S^0} \approx 1 + 6\text{Re}\frac{\epsilon'}{\epsilon},$$

where each  $N$  refers to the number of  $K_{L,S}$  decaying to two charged or neutral pions. The  $N_S$  numbers will evidently be much larger than the  $N_L$ ; thus, the statistical errors coming from them will be negligible

compared to those coming from the  $N_L$ . We thus have

$$\delta\left(\frac{\epsilon'}{\epsilon}\right) = \frac{1}{6}\sqrt{(\Delta N_L^\pm)^2 + (\Delta N_L^0)^2} = \frac{1}{6}\sqrt{\frac{1}{N_L^\pm} + \frac{1}{N_L^0}} = \frac{1}{6}\sqrt{\frac{3}{2N_L^0}},$$

since by isospin symmetry there are twice as many charged two-pion decays as neutral two pion decays.  $N_L^0$  is given by the  $\phi$  cross-section, times the integrated luminosity per year, times the efficiency for  $K_L$  tags, times  $BR(\phi \rightarrow K_L K_S)$ , times  $BR(K_L \rightarrow \pi^0 \pi^0)$ , times the number of  $K_L$ 's that are within the fiducial volume (i.e., that are detectable):

$$N_L^0 = 5 \mu\text{b} \times 10^{10} \mu\text{b}^{-1} \times 2/3 \times 0.34 \times 10^{-3} \times (1 - e^{-150/350}) = 4 \times 10^6,$$

which gives as claimed,

$$\delta\left(\frac{\epsilon'}{\epsilon}\right) = 1 \times 10^{-4}.$$

### 1. 3 Other CP violating process/decays

So far  $CP$  violation has only been seen in  $K_L$  decays ( $K_L \rightarrow \pi\pi$  and semileptonic decays). DAΦNE can look for  $K_S \rightarrow \pi^0 \pi^0 \pi^0$ , the counterpart to  $K_L \rightarrow \pi\pi$ . The branching ratio for this process is proportional to  $\epsilon + \epsilon'_{000}$  where  $\epsilon'_{000}$  is a quantity similar to  $\epsilon'$ , signalling direct  $CP$  violation. It is not as suppressed as the normal  $\epsilon'$ , perhaps a factor of twenty less. Nonetheless, as the expected BR is  $2 \times 10^{-9}$ , the whole signal will be at the 30 event level, and therefore there is here only the possibility to see the  $CP$  impurity of  $K_S$ , never observed before, not direct  $CP$  violation. The current limit on this BR is  $3.7 \times 10^{-5}$ . Another possibility is to look at the difference in rates between  $K_S \rightarrow \pi^+ l^- \nu$  and  $K_S \rightarrow \pi^- l^+ \nu$ , which is expected to be  $\sim 16 \times 10^{-4}$ , measurable in one year's running at DAΦNE, to an accuracy of  $\sim 4 \times 10^{-4}$ . Again this would be only a measurement of  $\epsilon$ , not  $\epsilon'$ , but the observation for the first time of  $CP$  violation in two new channels of  $K_S$  decay would be nonetheless of considerable interest.

Evidence for direct  $CP$  violation can be also be obtained from the decays of charged kaons which are copiously produced at DAΦNE.  $CP$  invariance requires equality of the partial rates for  $K^\pm \rightarrow \pi^\pm \pi^+ \pi^-$  ( $\tau^\pm$ ) and for  $K^\pm \rightarrow \pi^\pm \pi^0 \pi^0$  ( $\tau'^\pm$ ). One can improve the present rate asymmetry measurements by two orders of magnitude. One can also observe differences in the Dalitz plot distributions for  $K^+$  and  $K^-$  decays in both the  $\tau$  and  $\tau'$  modes; at DAΦNE one could reach sensitivities of  $\sim 10^{-4}$ . Finally, differences in rates in the radiative two pion decays of  $K^\pm$ ,  $K^\pm \rightarrow \pi^\pm \pi^0 \gamma$ , are also proof of direct  $CP$  violation. At DAΦNE the sensitivity reachable is  $\sim 1.4 \times 10^{-3}$ .

### 1. 4 Chiral perturbation theory

In the last decade chiral perturbation theory (CHPT) has been extended to the next order terms in the chiral expansion ( $\mathcal{O}(m^4)$ ,  $\mathcal{O}(p^4)$ ,  $\mathcal{O}(m^2 p^2)$ ). Many new amplitudes can then be predicted.<sup>[3]</sup> At lowest order the CHPT relation predicts the slope of the scalar form factor,  $\lambda_0$ . There is at present disagreement of experiment with the CHPT prediction,  $0.017 \pm 0.004$ . One can measure  $\lambda_0$  for  $K_L$  to an accuracy of  $1.4 \times 10^{-5}$ . Similar accuracies are obtainable for  $K^\pm$  and for  $\lambda_+$ . There is only one measurement of the relevant  $K_{\ell 4}$  form factors. These decays provide an unique opportunity for the determination of the  $\pi\pi$  phase shift.<sup>[4]</sup> The amplitudes for  $K_{\ell 2, \gamma}$ ,  $K_{\ell 2, e+e-}$  and  $K_{\ell 3, \gamma}$  depend on the  $K$  charge radius. The rate for  $K^\pm \rightarrow \pi^\pm \gamma\gamma$  and the  $\gamma\gamma$  distributions are uniquely predicted by the chiral lagrangian approach. Dalitz decays of  $K$  mesons and two photon production of pions are also of great interest.



### 1. 5 Radiative $\phi$ decays

Many other physics topics can be studied, especially at the DAΦNE start-up time, when the number of beam bunches will be approximately a quarter (30) of the final design value. An example is the study of light meson spectroscopy. Precise measurements of the  $\eta - \eta'$  mixing have important bearings on quark models and QCD, in particular on the question of whether there are gluonic components in the  $\eta$  and  $\eta'$  wave functions.<sup>[5]</sup> In this regard, measurements of the radiative  $\phi$  decays to  $\eta$  and to  $\eta'$ , which are feasible with great sensitivity using KLOE, can lead to a really decisive test, when combined with the information coming from other sources such as the analogous  $J/\Psi$  decays and the two-photon decays of  $\eta$  and  $\eta'$ . To complete the determination of the  $\eta'$  parameters we need measurements of the rare transition  $\phi \rightarrow \eta'\gamma$ . There is some room for a non-vanishing gluonic component in the  $\eta'$ . To give an idea of the expected order of magnitude of the branching ratio, for no gluonium in the  $\eta'$  and a mixing angle of  $20^\circ$  we expect  $\text{BR}(\phi \rightarrow \eta'\gamma) \sim 1.2 \times 10^{-4}$ . A Monte Carlo study<sup>[6]</sup> shows that KLOE can reach, during the commissioning year of DAΦNE, BR's of  $\sim 10^{-6}$ .

At the end of 1996, DAΦNE will begin delivering of the order of 500  $\phi$ -mesons/sec. This provides a unique opportunity to study the  $f_0(975)$  in  $\phi$  radiative decays, even for branching ratios which in some estimates could be as low as  $1 \times 10^{-6}$ . The unique, lightest scalar meson state  $f_0(975)$  is poorly described by current models. By Monte Carlo studies we show that the branching ratio above can easily be measured in the neutral decay channel  $f_0 \rightarrow \pi^0 \pi^0$ .<sup>[7]</sup> In decays to  $\pi^+ \pi^-$ , there are backgrounds from continuum processes.<sup>[8]</sup> Interference between one of these processes and the  $f_0$  amplitude leads to very interesting and complex patterns.<sup>[9]</sup> A complete study of the photon spectrum from  $e^+ e^- \rightarrow \pi^+ \pi^- \gamma$  at the  $\phi$  peak, after suppression of continuum contributions by suitable kinematics and angular cuts, can determine the sign of the  $\phi f_0 \gamma$  coupling even for the smallest branching ratio, thus providing a totally new piece of information for the investigation of the nature of the  $f_0$ .<sup>[7]</sup>

### 1. 6 $e^+ e^-$ annihilations into hadrons from threshold to 1.5 GeV

Precise measurements of  $\sigma(e^+ e^- \rightarrow \text{hadrons})$  up to energies of  $\sim 1.5$  GeV are necessary for the calculation of the muon anomaly  $a_\mu$ .<sup>[10]</sup> The required accuracy for the measurements<sup>[11]</sup> of  $\sigma(e^+ e^- \rightarrow \text{hadrons})$  is  $\sim 0.560\%$ , readily accessible to KLOE.

### 1. 7 Other decays

DAΦNE will be a unique source of pure  $K_S$ , thanks to tagging, providing up to  $10^{10}$  kaons per year, and allowing measurements of rare  $K_S$  decay modes, most of which have not been measured yet, down to the  $10^{-8}$  or  $10^{-9}$  level. Rare charged  $K$  decay modes will also be studied. It will be a place to study many rare decays, such as  $\phi \rightarrow \eta\gamma$ , and  $\eta$  decays. In table 1 some of the improvements that may be made in rare decay BR limits are listed.

Table 1. Rare decays.

Decay mode	To date	Limits that can be achieved at DAΦNE
$\eta \rightarrow 3\gamma$	$\text{BR} < 5 \times 10^{-4}$	$1.4 \times 10^{-8}$
$\eta \rightarrow \omega\gamma$	$\text{BR} < 5 \times 10^{-2}$	$10^{-9}$
$\phi \rightarrow \rho\gamma$	$\text{BR} < 2 \times 10^{-2}$	$10^{-9}$
$\phi \rightarrow \pi^+\pi^-\gamma$	$\text{BR} < 7 \times 10^{-3}$	$10^{-9}$
$\eta \rightarrow \pi^0 e^+ e^-$	$\text{BR} < 4 \times 10^{-5}$	$1.4 \times 10^{-8}$
$\eta \rightarrow \pi^0 \mu^+ \mu^-$	$\text{BR} < 5 \times 10^{-6}$	$1.4 \times 10^{-8}$

## 2 – The KLOE Design

The KLOE-Detector, with its distinctive logo, was proposed to the LNF's Scientific committee and given stage-I approval April 28, 1992.<sup>[12]</sup> A technical design proposal was submitted to the same committee on January 12, 1993.<sup>[13]</sup> It was fully approved on March 19, 1993. Two additional addenda were written to amplify design concerns specific to the central drift chamber,<sup>[14]</sup> and to the data acquisition system.<sup>[15]</sup> These four documents by the KLOE Collaboration are the source materials containing the full evolutionary details of the KLOE design. Here, I have extracted the salient features and the parameters of the main components of the final detector. I also list some of the interesting results obtained during our prototyping and test work, to give a flavor of how much has been achieved and what still remains to be done.

The KLOE detector requirements are:

1. Collect enough statistics
2. Measure the path length of the  $K_S$ ,  $K_L$  decays to the required accuracy
3. Reject backgrounds at the desired level
4. Be self-calibrating, using various  $K$  decay modes, in addition to Bhabha scattering events.

Its scale is driven by a fundamental parameter, the mean decay path length of the long lived  $K^0$ -meson  $L(K_L)$ : at DAΦNE,  $\beta(K)=0.216$  and  $L(K_L) = \gamma\beta c\tau = 3.44$  m.

### 2. 1 The KLOE Collaboration

The KLOE Collaboration has approximately 140 members from 10 Italian institutions supported by the INFN: Bari, Frascati, Lecce, Napoli, Pisa, Roma I, Roma II, Roma III, ISS Roma, Trieste/Udine, four foreign ones: IHEP at Beijing, Univ. of Karlsruhe, Columbia Univ. and SUNY at Stony Brook. The spokesman since its inception is Paolo Franzini. The individual name rosters as of December 1995 is listed below.

A. Aloisio,<sup>e</sup> A. Andryakov,<sup>b</sup> A. Antonelli,<sup>b</sup> M. Antonelli,<sup>b</sup> F. Anulli,<sup>b</sup> C. Avanzini,<sup>h</sup> D. Babusci,<sup>b</sup> C. Bacci,<sup>j</sup> R. Baldini-Ferroli,<sup>b</sup> G. Barbiellini,<sup>m</sup> K. Barth,<sup>c</sup> V. Baturin,<sup>e</sup> H. Beker,<sup>h</sup> G. Bellettini,<sup>g</sup> G. Bencivenni,<sup>b</sup> S. Bertolucci,<sup>b</sup> C. Bini,<sup>h</sup> C. Bloise,<sup>b</sup> V. Bocci,<sup>i</sup> F. Bossi,<sup>b</sup> P. Branchini,<sup>k</sup> L. Bucci,<sup>h</sup> A. Calcaterra,<sup>b</sup> R. Caloi,<sup>h</sup> P. Campana,<sup>b</sup> G. Capon,<sup>b</sup> M. Carboni,<sup>b</sup> G. Cataldi,<sup>d</sup> S. Cavaliere,<sup>e</sup> F. Ceradini,<sup>j</sup> L. Cerrito,<sup>i</sup> M. Cerù,<sup>h</sup> F. Cervelli,<sup>g</sup> F. Cevenini,<sup>e</sup> G. Chiefari,<sup>e</sup> G. Ciapetti,<sup>h</sup> M. Cordelli,<sup>b</sup> P. Creti,<sup>d</sup> A. Doria,<sup>e</sup> F. Donno,<sup>b</sup> R. De Sangro,<sup>b</sup> P. De Simone,<sup>b</sup> G. De Zorzi,<sup>h</sup> D. Della Volpe,<sup>e</sup> A. Denig,<sup>c</sup> G. Di Cosimo,<sup>h</sup> A. Di Domenico,<sup>h</sup> E. Drago,<sup>e</sup> V. Elia,<sup>d</sup> O. Erriquez,<sup>a</sup> A. Farilla,<sup>a</sup> G. Felici,<sup>b</sup> A. Ferrari,<sup>g</sup> M. L. Ferrer,<sup>b</sup> G. Finocchiaro,<sup>b</sup> D. Fiore,<sup>e</sup> P. Franzini,<sup>h,j</sup> A. Gaddi,<sup>b</sup>

C. Gatto,<sup>e</sup> P. Gauzzi,<sup>h</sup> E. Gero,<sup>b</sup> S. Giovanella,<sup>h</sup> V. Golovyatuk,<sup>d</sup> E. Gorini,<sup>d</sup> F. Grancagnolo,<sup>d</sup> W. Grandegger,<sup>b</sup> E. Graziani,<sup>k</sup> U. v. Hagel,<sup>c</sup> M. Imhof,<sup>c</sup> M. Incagli,<sup>g</sup> C. Joram,<sup>c</sup> L. Keeble,<sup>b</sup> W. Kim,<sup>l</sup> W. Kluge,<sup>c</sup> F. Lacava,<sup>h</sup> G. Lanfranchi,<sup>h</sup> P. Laurelli,<sup>b</sup> J. Lee-Franzini,<sup>b,l</sup> A. Martini,<sup>b</sup> A. Martinis,<sup>m</sup> M. M. Massai,<sup>g</sup> R. Messi,<sup>i</sup> L. Merola,<sup>c</sup> A. Michetti,<sup>h</sup> S. Miscetti,<sup>b</sup> S. Moccia,<sup>b</sup> F. Murtas,<sup>b</sup> M. Napolitano,<sup>c</sup> A. Nisati,<sup>h</sup> E. Pace,<sup>b</sup> G. F. Palamà,<sup>d</sup> M. Panareo,<sup>d</sup> L. Paoluzi,<sup>i</sup> A. Parri,<sup>b</sup> E. Pasqualucci,<sup>i</sup> M. Passaseo,<sup>h</sup> A. Passeri,<sup>k</sup> V. Patera,<sup>b</sup> F. Pelucchi,<sup>b</sup> E. Petrolo,<sup>h</sup> M. C. Petrucci,<sup>h</sup> M. Piccolo,<sup>b</sup> M. Pollack,<sup>l</sup> L. Pontecorvo,<sup>h</sup> M. Primavera,<sup>d</sup> F. Ruggieri,<sup>a</sup> P. Santantonio,<sup>b</sup> R. D. Schamberger,<sup>l</sup> A. Sciubba,<sup>h</sup> F. Scuri,<sup>m</sup> A. Smilzo,<sup>e</sup> S. Spagnolo,<sup>d</sup> E. Spiriti,<sup>k</sup> C. Stanescu,<sup>k</sup> L. Tortora,<sup>k</sup> P. M. Tuts,<sup>l</sup> E. Valente,<sup>h</sup> P. Valente,<sup>b</sup> G. Venanzoni,<sup>g</sup> S. Veneziano,<sup>h</sup> S. Weseler,<sup>c</sup> R. Wieser,<sup>c</sup> S. Wölflé,<sup>b</sup> Y. G. Xie,<sup>n</sup> A. Zallo,<sup>b</sup> C. D. Zhang,<sup>n</sup> J. Q. Zhang,<sup>n</sup>

<sup>a</sup> Dipartimento di Fisica dell'Università e Sezione INFN, Bari

<sup>b</sup> Laboratori Nazionali di Frascati dell'INFN, Frascati

<sup>c</sup> Institut für Experimentelle Kernphysik, Universität Karlsruhe

<sup>d</sup> Dipartimento di Fisica dell'Università e Sezione INFN, Lecce

<sup>e</sup> Dipartimento di Scienze Fisiche dell'Università e Sezione INFN, Napoli

<sup>f</sup> Physics Department, Columbia University, New York

<sup>g</sup> Dipartimento di Fisica dell'Università e Sezione INFN, Pisa

<sup>h</sup> Dipartimento di Fisica dell'Università e Sezione INFN, Roma I

<sup>i</sup> Dipartimento di Fisica dell'Università e Sezione INFN, Roma II

<sup>j</sup> Dipartimento di Fisica dell'Università di Roma III e Sezione INFN, Roma I

<sup>k</sup> Istituto Superiore di Sanità and Sezione INFN, ISS, Roma.

<sup>l</sup> Physics Department, State University of New York at Stony Brook

<sup>m</sup> Dipartimento di Fisica dell'Università e Sezione INFN, Trieste/Udine

<sup>n</sup> Institute of High Energy Physics of Accademia Sinica, Beijing, China

## 2. 2 Systematics constraints

Since the observation<sup>[16]</sup> in 1964 that the long lived  $K^0$  meson decays into two pions, the search for direct  $CP$  violation has failed. In terms of physical observables, if the direct  $CP$  violating amplitude  $\langle \pi\pi | K_2 \rangle$ , where  $K_2$  is  $CP$ -odd, vanishes, then:

$$\mathcal{R}_S \equiv \frac{\Gamma(K_S \rightarrow \pi^+\pi^-)}{\Gamma(K_S \rightarrow \pi^0\pi^0)} = \mathcal{R}_L \equiv \frac{\Gamma(K_L \rightarrow \pi^+\pi^-)}{\Gamma(K_L \rightarrow \pi^0\pi^0)},$$

otherwise, in general,  $|\mathcal{R}_S - \mathcal{R}_L| = \Delta\mathcal{R} \neq 0$  and  $|\Delta\mathcal{R}/\mathcal{R}| = 6 \times |\text{Re}(\epsilon'/\epsilon)|$ .

The aim of KLOE is to reach a sensitivity in  $\Delta\mathcal{R}/\mathcal{R}$  of  $\sim 6 \times 10^{-4}$ , which from the statistical point of view, is achievable at DAΦNE at full luminosity in about one year. The two formidable tasks for KLOE to face are the controlling of efficiencies for the decays of interest and the rejection of background from the copious  $K_L$  decays to states other than two pions. The relation between measurements and BR's, assuming tagging is used, is:

$$\underbrace{N_{L,S}^{\pm,0}}_{\text{observed}} - \underbrace{BK_{L,S}^{\pm,0}}_{\text{estimated}} = \underbrace{N_{KK} \times \varrho_{L,S}(\text{tag})}_{\text{cancels in ratio}} \times \underbrace{BR_{L,S}^{\pm,0}}_{\text{desired}} \times \underbrace{\langle \varrho_{L,S}^{\pm,0} \rangle}_{\text{(efficiency)}} \\ \times \iint_{\text{FV}} g(l-l') I(l) dl dl'.$$

The double integral is a convolution of the decay intensity  $I(l)$  and the experimental resolution  $g(l-l')$  in the measurement of the decay path length and an integration over the fiducial volume, FV, of the

detector. The four backgrounds  $BK_{L,S}^{\pm,0}$  and the averaged efficiencies  $\langle \epsilon_{L,S}^{\pm,0} \rangle$  are different. They must be known to an accuracy of  $\mathcal{O}(1/3000)$ .

### 2.3 Fiducial volumes

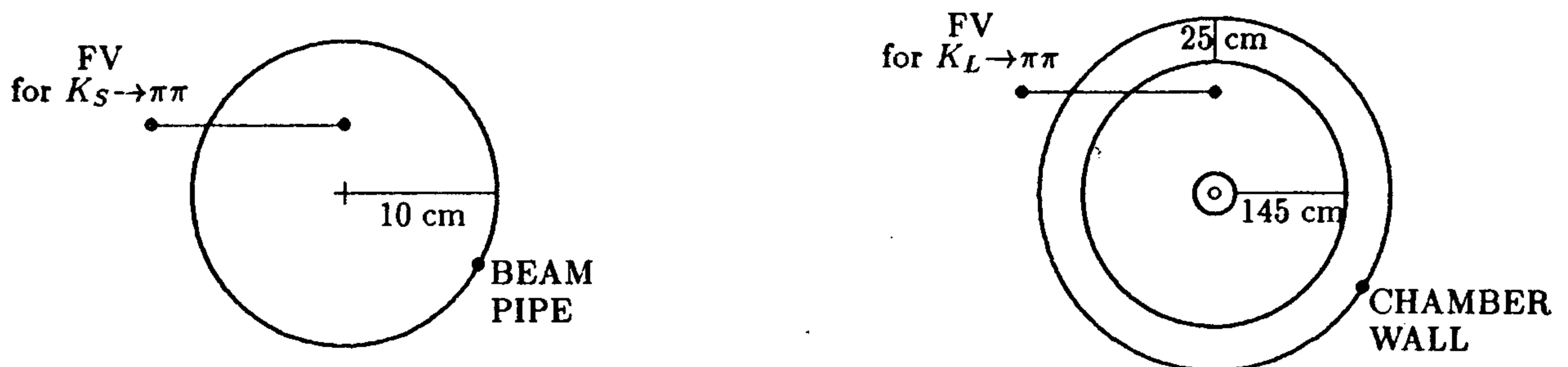


Fig. 9. Fiducial Volumes for  $K_S$  and  $K_L$  decays.

As will be described later, our detector consists of an electromagnetic calorimeter, a large tracking chamber and a vertex detector. The calorimeter has a central part which is a cylinder of 2 m radius and 3.5 m length, closed by two end caps, covering  $\sim 98\%$  of the solid angle. The chamber, with inner wall of 25 cm radius, provides tracking for  $30 < r < 200$  cm. The whole detector is immersed in a solenoidal field of 0.6 T. Regeneration in walls (beam pipe, chamber walls) is  $\leq 1\%$ . Use of a large beam pipe, 10 cm radius, inside which all  $K_S$ 's decay, and rejection of  $K$  decays up to 6 cm ( $10 \tau_S$ ) past any wall eliminate the effects of  $K_L \rightarrow K_S$  regeneration. The fiducial volume (FV) for  $K_S$  and  $K_L$  decays are idealized in fig. 9. The fiducial volume for  $K_L$  decays, in cylindrical coordinates, is taken as:

$$\begin{aligned} 30 < r < 175 \text{ cm} \\ -125 < z < 125 \text{ cm} \end{aligned}$$

If the integral over the FV equation could be carried out to infinity, FV boundary and resolution would not contribute any error. This is essentially the case for  $K_S$  decays. A  $K_L$  signal guarantees the presence of a  $K_S$ . The beam pipe has radius equivalent to  $\geq 13$ – $17$  lifetimes. Therefore without imposing, ideally, any fiducial volume cut on the data, the integrals are "1", independently of flight path resolution. Efficiencies for  $\pi^+\pi^-$  and  $\pi^0\pi^0$  decays are  $\geq 99\%$  and are well-controlled. Backgrounds are at the level of  $10^{-3}$ , before any cuts are applied.

The case is quite different for  $K_L$  decays, since the fiducial volume has dimensions,  $\sim 145$  cm, which are about half the mean decay path of  $\sim 350$  cm. A small error on the determination of the boundary of the fiducial volume can introduce large errors on  $\mathcal{R}_L$ , at the accuracy of interest. What is relevant is the relative error in the determination of the boundaries of the fiducial volumes for  $K_L \rightarrow \pi^+\pi^-$  and  $K_L \rightarrow \pi^0\pi^0$ , since different methods are used to obtain the  $K_L$  path length.  $K_L \rightarrow K_S$  regeneration at the chamber's inner wall provides in fact an excellent check of the correct knowledge of the inner boundary of the fiducial volumes. To achieve a sensitivity of  $6 \times 10^{-4}$  in  $\Delta \mathcal{R} / \mathcal{R}$ , we must insure that the outer boundaries of the fiducial volumes for charged and neutral decays are equal to better than 0.5 mm. The most effective way to ensure this is to use  $K_L$  decays for which both a "neutral" and a "charged" decay vertex is measurable, such as  $K_L \rightarrow \pi^+\pi^-\pi^0$ . Decays of charged  $K$ 's,  $K^\pm \rightarrow \pi^\pm\pi^0$ , can also be used over part of the FV.

## 2. 4 Backgrounds

The main sources of background in  $CP$  experiments are the non- $CP$  violating decays of  $K_L$ ,  $\pi^0\pi^0\pi^0$ ,  $\pi^+\pi^-\pi^0$ ,  $K_{\mu 3}$ , and  $K_{e3}$ ,  $\sim 100$  times more abundant than the  $CP$ -violating modes. The rejection of  $\pi^0\pi^0\pi^0$  relies on good solid angle coverage and efficiency for  $\gamma$ 's down to 20 MeV energy, which we will achieve in correct calorimeter design. The rejection of  $\pi^+\pi^-\pi^0$  is easier because the probability of losing 2/2  $\gamma$ 's is 15 times smaller than losing 2/6  $\gamma$ 's; in addition, we will have help from chamber measurements of the charged tracks.

A realistic study of the methods for removing  $K_{\mu 3}$  contamination has been developed. A large sample,  $1.35 \times 10^7$   $K_{\mu 3}$  and  $10^5$   $K_L \rightarrow \pi^+\pi^-$  events, was generated using the standard size of the luminous region,  $\sigma_x = 0.2$  cm,  $\sigma_y = 20$   $\mu$ m,  $\sigma_z = 3$  cm.  $K \rightarrow K_{\mu 3}$  and  $K \rightarrow \pi^+\pi^-$  events are distinguished by the use of a  $\chi^2$  function constructed using the measured variables corresponding to all the kinematical constraints available. A double Gaussian parameterization has been applied to the resolution functions (in  $p_T$ ,  $\phi$ ,  $\cot(\theta)$ , vertex position) obtained from reconstructed GEANFI<sup>[17]</sup> generated tracks, using the ARGUS-KLOE program for a 84 layer stereo chamber, to take tails into account. The  $\chi^2$  function is peaked at very low values for  $K_L \rightarrow \pi^+\pi^-$  decays, while for  $K_{\mu 3}$  events it vanishes at 0 and extends to very high values. This calculation has been repeated for several values of the magnetic field, 4 to 8 kG. The rejection factor at 6 kG is approximately  $4.5 \times 10^{-4}$  with a  $\pi^+\pi^-$  signal efficiency of 98.8%.<sup>[14]</sup> The  $K_{e3}$  decays are more easily distinguished and removed, partly because  $m_e \ll m_\mu$ , and the energy deposition pattern of an electromagnetic shower in the calorimeter is very distinctive.

## 2. 5 Trigger

Triggering at DAΦNE will be an entirely new experience. At full luminosity, the  $\phi$ -event rate is  $\sim 5$  kHz while the machine produced background when properly masked, can be estimated, scaling from other machines, to be  $\sim 10\%$  of this value. All events in principle must be passed to the digitizing electronics (FEE) and data acquisition system (DAQ). The calorimeter can provide an adequate trigger for most events of interest, especially when complemented with some tracking information. Bhabha scattering at angles  $10^\circ < \theta < 20^\circ$  and cosmic ray events must be recognized and rejected or prescaled not to overload FEE and DAQ. Both these two classes of events are important for detector calibration. We will employ calorimeter information and simple combinatorial logic to reject/scale these events.

## 2. 6 Calibration

At DAΦNE a general purpose detector capable of measuring all decay modes of the  $\phi$  has a wealth of processes useful for the calibration of its efficiencies. Furthermore the availability of abundant Bhabha scatterings observed in the detector allows a complete calibration of energy and time scales. The following table summarizes the accuracies to which the key parameters can be monitored by various methods. We conclude that KLOE is truly a "self-calibrating" detector!

Table 2. Detector Calibration

Parameter	Method, Process	Accuracy/m
Energy Scale	Continuous, absolute: BHABHA	1%/cluster
Time Scale	- same - : BHABHA	12ps/cluster
Tracking Efficiency	- same - : $e^+e^-$ , $\mu^+\mu^-$ , $K \rightarrow 3\text{body}$	$10^{-3}$ /track
Photon Efficiency	- same - : $K^\pm \rightarrow \pi^\pm\pi^0$ , $K^0 \rightarrow \pi^+\pi^-\pi^0$	$10^{-3}$ /cluster
F.V. $\pi^0\pi^0/\pi^+\pi^-$	Cont., relative: $K^\pm \rightarrow \pi^\pm\pi^0$ , $K^0 \rightarrow \pi^+\pi^-\pi^0$	$10^{-3}$ /global

### 3 – The KLOE Detector

From the discussions of the previous section we conclude that KLOE must be able to track charged particles of momenta between 50 and 250 MeV/c. It must also detect with very high efficiency  $\gamma$ 's with energy as low as 20 MeV, measure their energies with a resolution  $\delta E_\gamma/E_\gamma \sim 15\%$  at 100 MeV, and provide the space coordinates of the photon conversion point so that the  $K_L$  decay path can be determined to within  $\sim 1$  cm. Thus while the general features of the KLOE detector are similar to those of a *typical* general purpose collider's apparatus: a cylindrical structure surrounding the beam pipe, consisting of a highly efficient, large tracking device for detecting the charged  $K^0$  decay products, an electromagnetic calorimeter with exceptional timing ability, which also provides some particle identification, all enclosed in a solenoidal field, each component has its own unusual features. The KLOE cross section is shown in fig. 10. The radius of the beam pipe around the luminous point is 10 cm. This allows the definition of a fiducial region for  $K_S$  decays without complication from regeneration. The beam pipe is made of 0.5 mm thick beryllium to minimize multiple scattering, energy loss for charged kaons and regeneration. The enlargement of the beam pipe at the interaction point, is a technical challenge for DAΦNE because it could act as a free wheeling RF cavity, with all the attending problems. In figure 10 we also show that the low  $\beta$  insertion permanent magnets are mounted directly on the beam pipe, inside KLOE, another difficult technical problem to be solved.

### 4 – Central Tracking Chamber

The design of the large tracking chamber for the KLOE detector is driven for the most part by the following considerations:

1. Maximize the homogeneity and isotropy of the active tracking volume because of the long decay path of the  $K_L$  and the isotropic angular distribution of the charged decay products.
2. Achieve a high and a well-controlled efficiency for the reconstruction of  $K_L \rightarrow \pi^+\pi^-$  decays.
3. Maximize, without forgetting the points above, the fiducial volume for decay detection, to obtain the largest event sample for a given delivered luminosity.
4. Optimize resolution at low momentum values.
5. Minimize the number of wires, both sense and field, in order to ease the difficulties of building a transparent chamber shell, minimize multiple scattering and maintain the electronics channels count within reasonable limits.

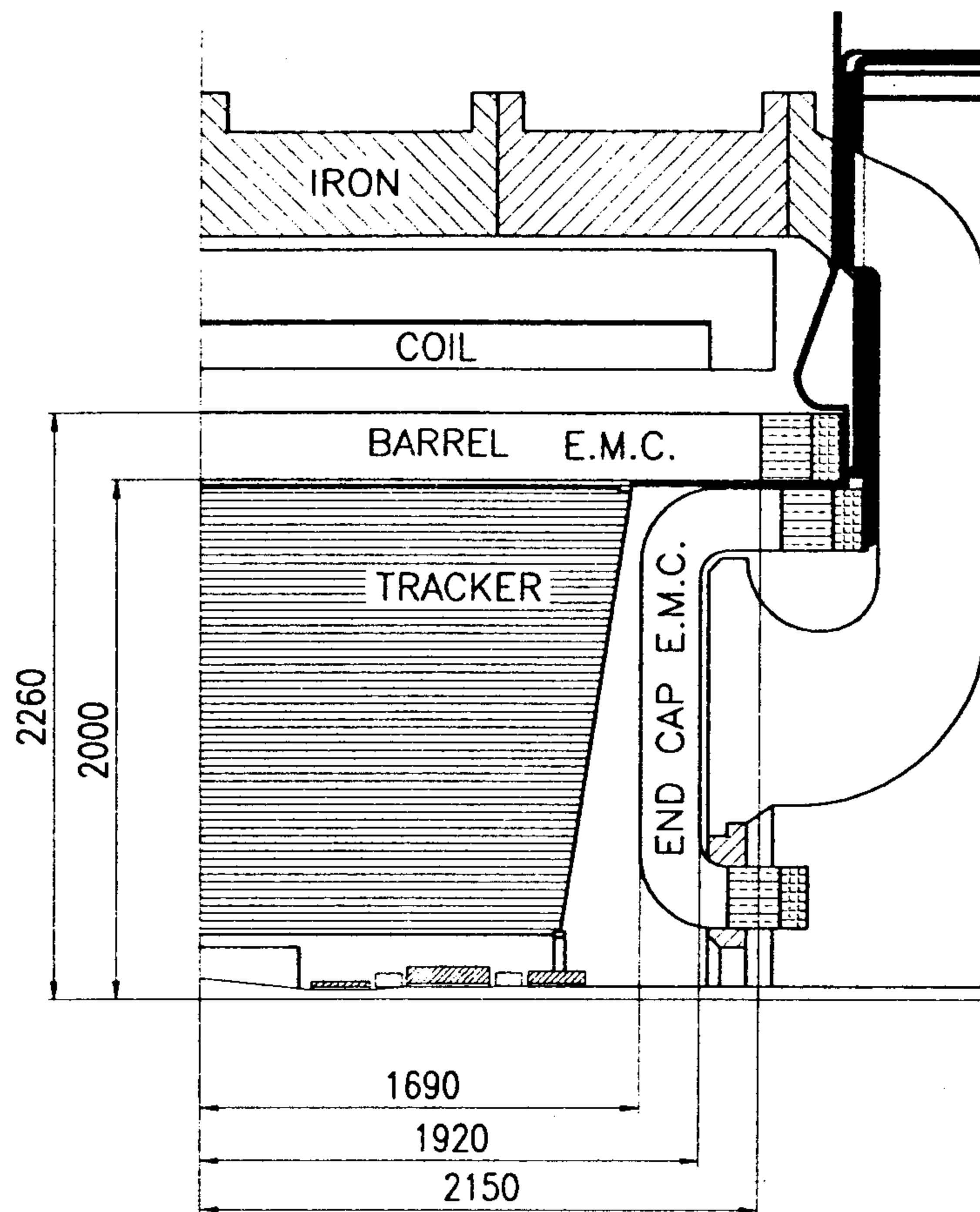


Fig. 10. KLOE cross section along the beam axis.

The decay length of  $K_L$ 's,  $\lambda_D=350$  cm, requires that a long decay path be available to observe a significant fraction of their decays. A reasonable compromise is to detect  $K_L$  decays in a big, cylindrical chamber of radius  $\sim 2$  m and length 370 cm. The above tracking volume is located inside a  $15 X_0$  thick, lead-scintillating fiber e.m.calorimeter, surrounded in turn by a superconducting coil providing a solenoidal field of 0.6 T.

The quasi uniform distribution of  $K_L$  decay vertices and secondary tracks in the chamber volume requires a constant size drift cell. This is achieved by using only alternating stereo layers, with constant inward radial displacement at the chamber center, resulting in a stereo angle which increases with radius, in KLOE  $50 \text{ mrad} \leq \theta_{st} \leq 120 \text{ mrad}$ , and an approximately constant, square cell shape along  $z$ , with constant wire gain. An optimal configuration, assuring good tracking also for  $K_S \rightarrow \pi^+ \pi^-$  decays, might consist of twelve layers in the inner part of the chamber with  $1.5 \times 1.5 \text{ cm}^2$  cells, followed by  $3 \times 3$  cells. The number of cell layers for this case is 61 for a total number of cells of  $\sim 13,000$ .

Because of the low momenta of the decay products,  $<300$  MeV, we choose helium-based gas mixtures to minimize multiple scattering. A satisfactory choice is a 90-10 mixture of He- $iC_4H_{10}$  whose radiation length is  $X_0=1300$  m. The wires, W for sense and Al for field, result in a final value  $X_0=900$  m. Also, the choice of a relatively big drift cell of  $3 \times 3 \text{ cm}^2$  helps in reducing the total amount of material in the chamber, while still maintaining a proper time-space correlation over most of the cell. Drift velocity is generally not saturated. For an expected resolution on any single measurement of  $\sigma_{r\phi} \leq 200 \mu\text{m}$ ,

the  $K_L \rightarrow \pi^+ \pi^-$  vertex is expected to be reconstructed with accuracies  $\sigma_{x,y} \leq 500 \mu\text{m}$ ,  $\sigma_z \leq 1-2 \text{ mm}$ . The resolution for the reconstructed  $K_L$  mass is  $\sigma_M \sim 1 \text{ MeV}$ . The low drift velocity of He gas mixtures, and the smallness of the Lorentz angle, implies that the magnetic field will only change the time-space correlation without loss in either resolution or efficiency. This was confirmed during a beam test using a drift chamber prototype located inside a magnet, which could produce a field of 0.6 T, exposed to a beam at CERN. The effect of the magnetic field is measured to be small ( $\approx 5 \div 10\%$  change in drift velocity).

#### 4. 1 Mechanical structure

The KLOE chamber needs all its walls and the preamplifiers mounted on the chamber end plates to have the smallest possible thickness, in order to minimize photon conversions before the electromagnetic calorimeter as well as multiple scattering and energy losses of charged particles entering the chamber. The end plates of the KLOE chamber are spherical, kept apart by twelve rods attached to an outer ring. The plate deformation under load is strongly helped by properly attaching the plate outer rim to a torsionally stiff ring. Gas seal is completed by twelve panels which will be mounted after chamber stringing and an inner cylinder is attached to the end plates via two rings at the center of the plates which also provide support for the low  $\beta$  insertion. Panels and inner cylinder carry no loads in our chamber design. The mechanical structure of the drift chamber, with spherical end plates, can withstand without deformation the tension of some 50,000 wires with good transparency ( $\leq 0.1X_0$ ) to photons from  $\pi^0$  decays, to be detected in the calorimeter.

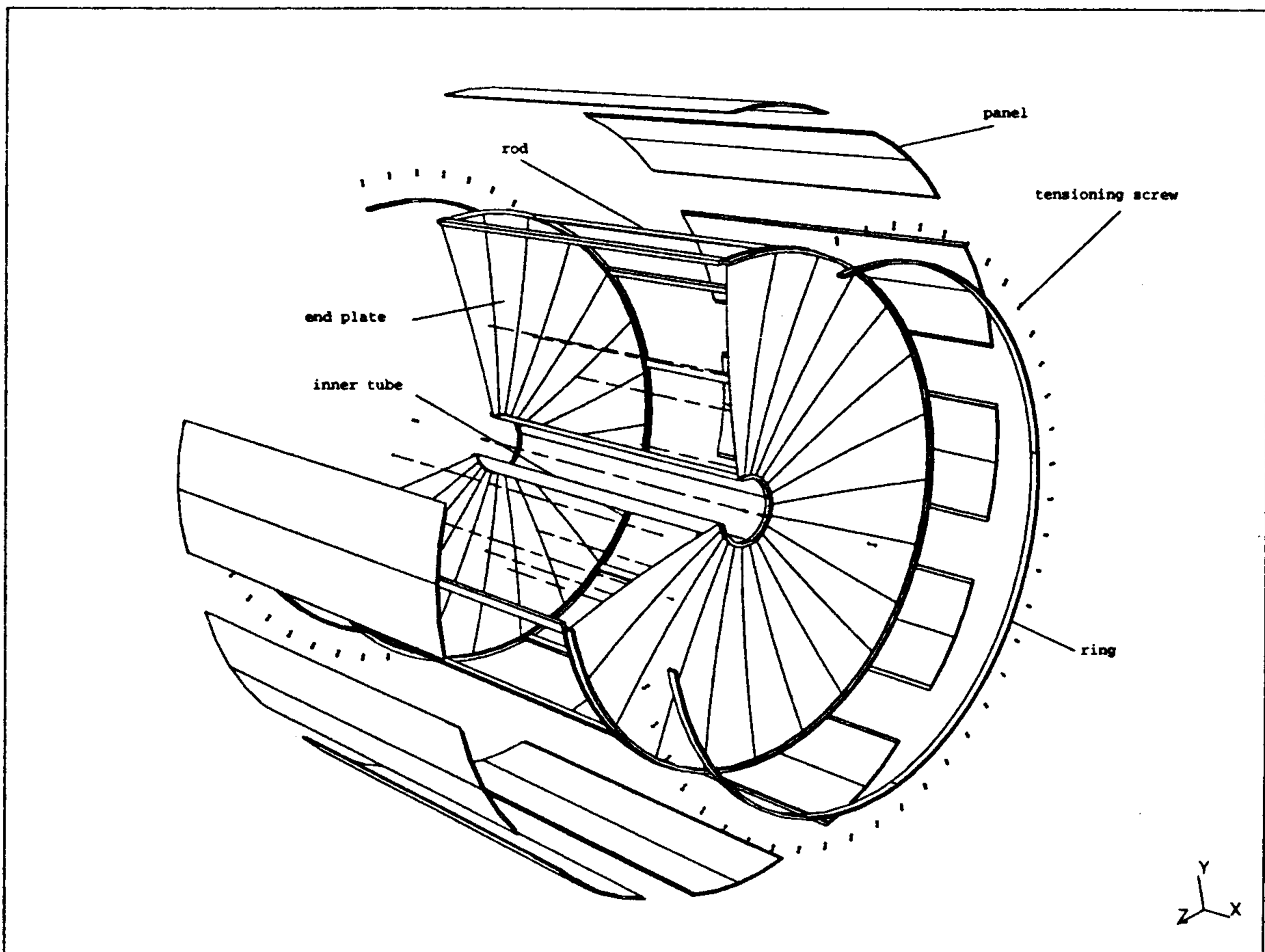


Fig. 11. Exploded View of the KLOE Chamber.



#### 4. 2 Prototype 1

In order to acquire first hand experience about all problems concerning materials, stringing procedure, gas tightness, signal and HV, etc. we have built a full length sector. The prototype, built with carbon fiber plates furnished by STESALIT A. G. of Zullwil, Switzerland, is 3.2 m long with 1 m<sup>2</sup> end plates. Five hundred single sense wire square cells, 3cm by 3cm and 1.5cm by 1.5cm, arranged in thirty layers, are strung at stereo angles in the range 50-120 mrad between two conical shaped carbon fiber end-plates.<sup>[18]</sup> Cosmic ray and beam test results confirm that it is invaluable for acquiring experience about all phases of the project.

#### 4. 3 Chamber parameters

The performance required of the KLOE tracking device is given below:

Table 3. Central Chamber Performance.

Drift Chamber, He gas mix, thin walls
$\delta_{\text{point}} = 200 \mu\text{m}, r \text{ and } \phi$
$= 2 \text{ mm}, z$
$\delta p_t = 0.5\% \times p_t$
$\delta(\tan(\theta)) = (3.5 \oplus 2.5) \times 10^{-4}$

### 5 – Calorimeter

Reconstruction of the  $\pi^0\pi^0$  decay mode of a 110 MeV/c momentum  $K$ , the determination of its decay point and the efficient rejection of the three  $\pi^0$  decays make designing the electromagnetic calorimeter, EmC, a most challenging project. Unique to the KLOE experiment, is the method of determining the flight path of  $K_L$ , the segment ID in fig. 12, by time measurements. I is the  $\phi$  decay point, the direction of ID is given by  $-\mathbf{p}_{K_S}$ , and A is the photon conversion apex in the calorimeter. As illustrated in fig. 12, the flight time measurements for even a single photon of the four from  $\pi^0\pi^0$  allow the determination of the  $K_L$  decay path. The time of arrival of a photon gives the flight path of the  $K^0$  to an accuracy  $\delta l = \beta_{K^0} c \delta t \sim 6 \times 10^{-3} \text{ cm} \times \delta t(\text{ps})$ . For a 510 MeV  $K^0$ , that is for four photons with  $\sum E_\gamma = 510 \text{ MeV}$ , one expects a time resolution of  $\sim 100 \text{ ps}$  and a path resolution of 0.6 cm. Observation of only three out of four photons still allows an over-constrained determination of both the  $K^0$  mass and the flight path, using time, position and energy measurements.

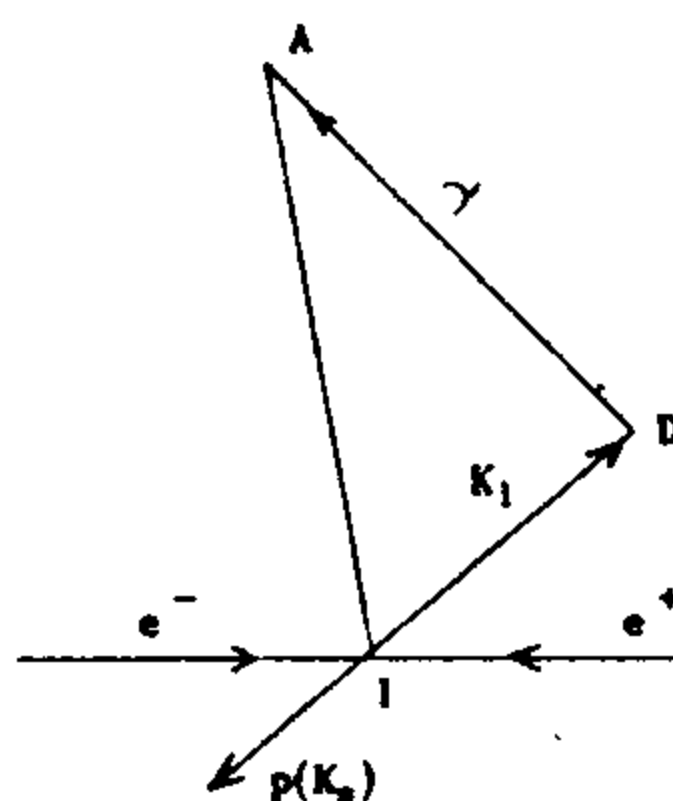


Fig. 12. Measuring the  $K_L$  decay length.

The KLOE EmC is a very fine sampling lead-scintillating fiber calorimeter, with photomultipliers (PMs) read-out. The central part, barrel, approximates a cylindrical shell of 4 m inner diameter, 4.3 m

active length and 23 cm thickness. The barrel covers the polar angle region  $49^\circ < \theta < 131^\circ$  and consists of 24 sectors with trapezoidal cross section,  $\sim 60$  cm wide. Two end-caps, 4 m in diameter and 23 cm thick, close hermetically the calorimeter. Each end-cap consists of 26 "C" shaped modules which run vertically along the chords of the circle inscribed in the barrel. At the two ends they are bent at  $90^\circ$ , becoming parallel to the barrel ends, to decrease the effects of the magnetic field on the PMs and to increase hermeticity, see figures 10 and 13. Partial KLOE views are shown in figure 13. The top figure shows an endview of the top half with half of the return iron yoke cut away, the lower figure shows a side view, again with half of the iron yoke cut away.

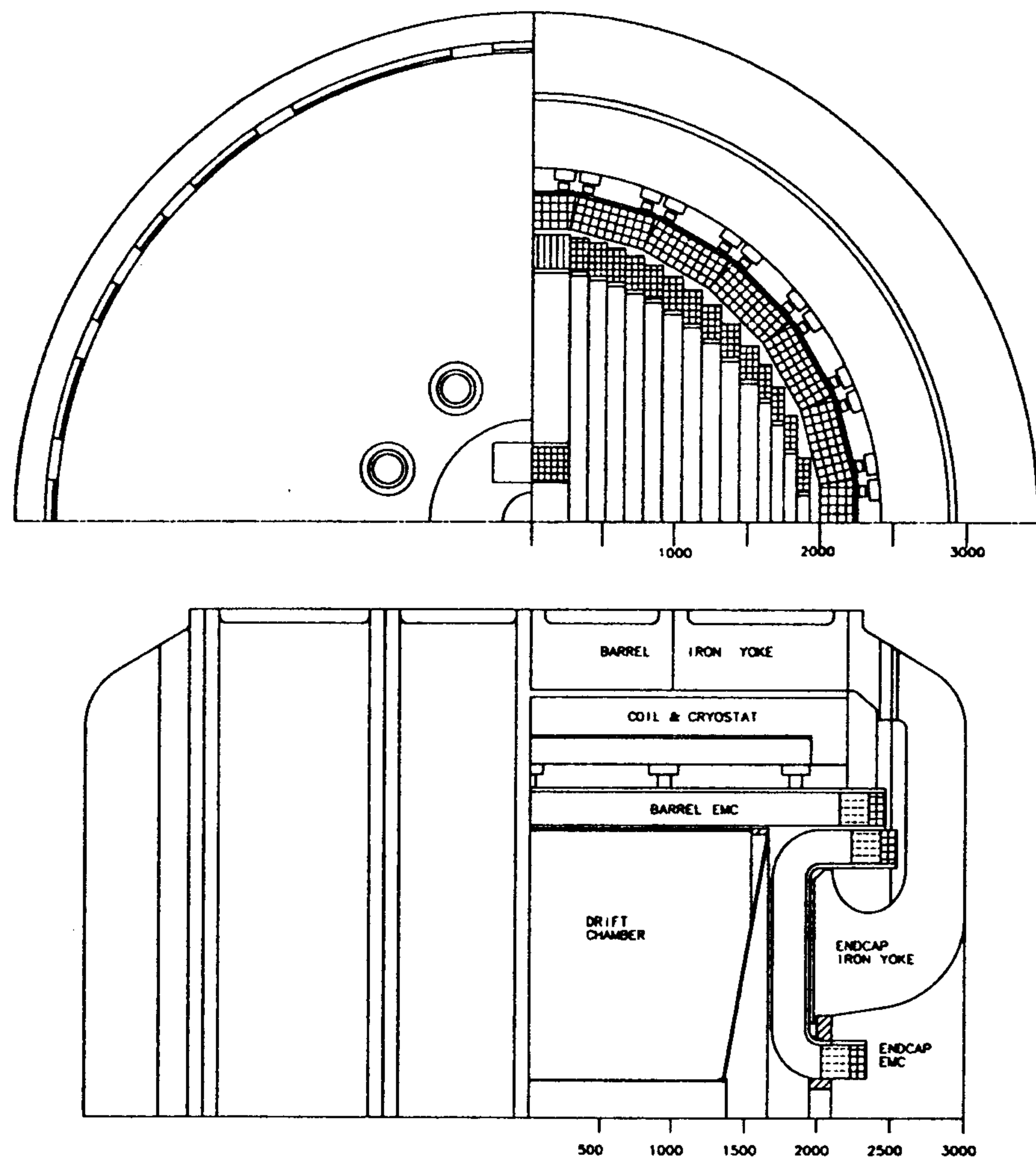


Fig. 13. Partial KLOE views.

In our EmC fibers run mostly transversely to the particle trajectories. This reduces sampling fluctuations due to channeling, resulting in improved resolution particularly important at low energies. Each module of the KLOE EmC is built by glueing 1 mm diameter blue scintillating fibers between thin grooved lead plates, obtained by passing 0.5 mm thick lead foils through rollers of proper shape. The grooves in the two sides of the lead are displaced by one half of the pitch so that fibers are located at the corners of adjacent, quasi-equilateral triangles resulting in optimal uniformity of the final stack, see fig. 14. The grooves are just big enough to insure that the lead does not apply direct pressure on the fibers. Light travelling in the cladding is effectively removed because of the glue surrounding the fibers. The

selected fiber pitch of 1.35 mm results in a structure which has a fiber:lead:glue volume ratio of 48:42:10 and a sampling fraction of  $\sim 15\%$  for a minimum ionizing particle. The final composite has a density of  $\sim 5 \text{ g/cm}^3$  and a radiation length  $X_0$  of  $\sim 1.6 \text{ cm}$ , is self-supporting, and can be easily machined. The very small lead foil thickness ( $< 0.1 X_0$ ) results in a quasi-homogeneous structure and in high efficiency for low energy photons. Measurements indicate that the blue-green Kuraray SCSF-81, Bicron BCF-12 and Pol.Hi.Tech-46 fiber, satisfy our requirements for light yield, scintillation decay time and attenuation length.<sup>[19]</sup> Since the time resolution depends on the light yield, great care has been put in maximizing the efficiency of the light collection system and insuring uniform photocathode illumination. Each light guide consists of a mixing part and a Winston cone concentrator.<sup>[20]</sup> We are thus able to match the calorimeter elements to the PM photocathodes, with an area reduction factor of up to  $\sim 4$ , without losses, because of the small  $22^\circ$  divergence angle of the light travelling in the fibers.

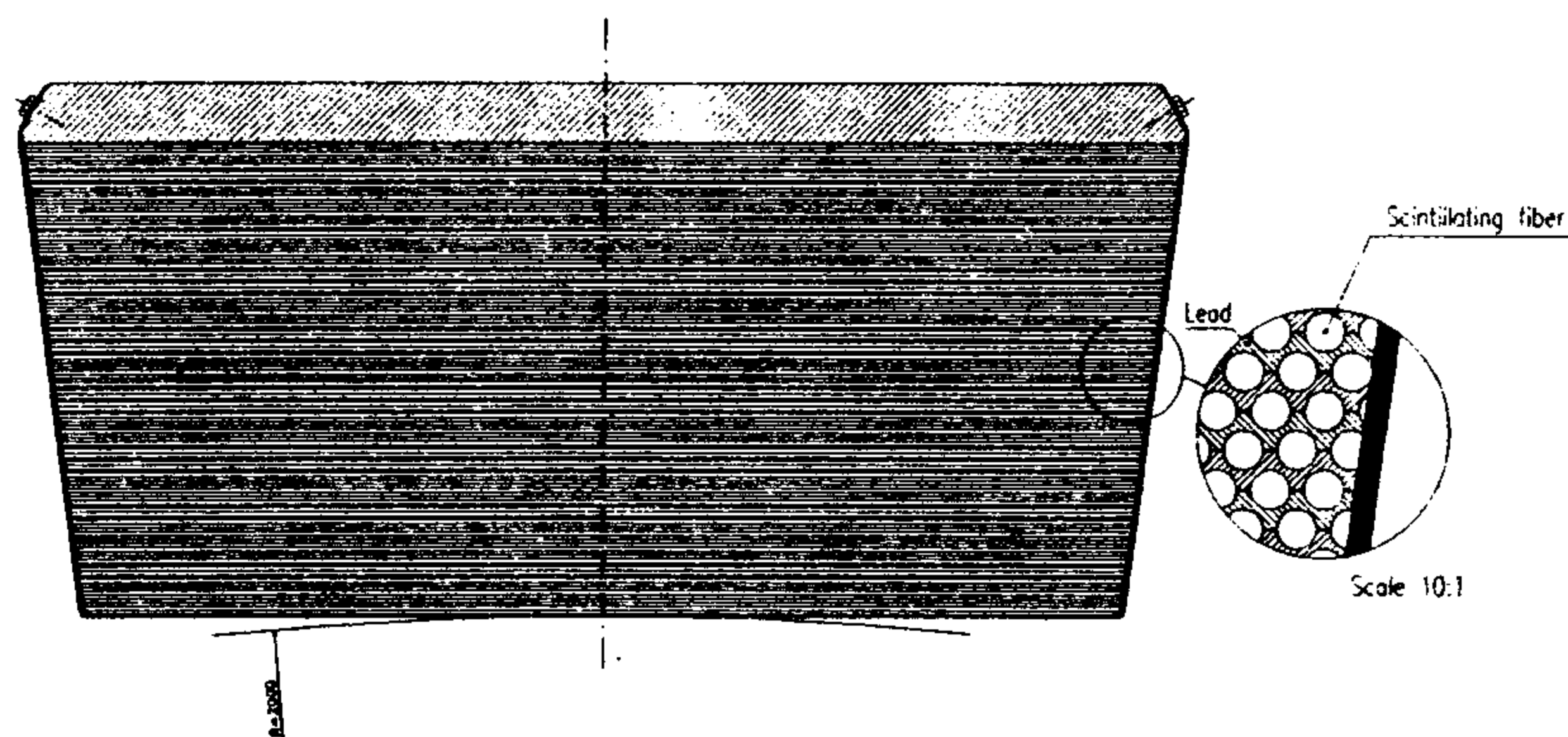


Fig. 14. Fiber and lead layout.

### 5. 1 Module IHEP

All the machinery for building the *barrel* calorimeter have been designed and built by the KLOE calorimeter group, mostly at LNF. The first full size *barrel* module, with dimensions of  $23 \text{ cm} \times 60 \text{ cm} \times 430 \text{ cm}$  and trapezoidal cross section, called module IHEP, was then successfully built, also at Frascati. The machinery has been turned over to a company which will assemble all modules of the *barrel* calorimeter. The front half of module IHEP is built with Kuraray SCSF-81 fibers and the back half with Pol.Hi.Tech-46 fibers.

The module read-out consists of five planes of 12 elements each, of  $\sim 4.4 \times 4.4 \text{ cm}^2$ , varying slowly in size across the module face. Each element is viewed through light pipes which provide mixing and terminate with a Winston concentrator coupled to mesh photomultipliers. The PMs are manufactured to KLOE specifications by Hamamatsu (R2021, mod.). KLOE needs to use these special tubes because they can operate in moderate magnetic field.<sup>[21]</sup> As shown in fig. 10, they are inside the return yoke where they see up to 0.15 T inclined less than  $25^\circ$  with respect to the PM's axis.<sup>[22]</sup> These PMs have a measured quantum efficiency of only  $\sim 60\%$  of the conventional tubes like the ones used in the previous prototypes.<sup>[23]</sup>

Module IHEP employs the final KLOE electronics. The PM base contains the voltage divider for the PMs working with grounded cathode to allow grounding of the tube shieldings and an A.C. coupled preamp which drives the cables carrying the signals outside of the magnet yoke. The signals enter three way splitters, providing input to a constant fraction discriminator, a driver for amplitude measurements and first level analog sums for trigger generation. All these functions are mounted on a 9U VME card,

containing 30 complete channels. Signals from this card go to the KLOE designed 12 bit ADC's,  $2\text{ V} \times 10\text{ ns}$  full scale, and 12 bit TDC's, 25 ps per count.<sup>[15]</sup> A description of KLOE electronics can be found in ref. 15.

Module IHEP was exposed to a test beam at PSI in July 1994. Analysis of the collected data is underway. Preliminary results indicate that  $\sigma_E/E \sim 5\%/\sqrt{E\text{ (GeV)}}$  and  $\sigma_T \sim 60\text{ps}/\sqrt{E\text{ (GeV)}}$ . These results are precisely the expected resolutions taking into account the length of the full module (4.3 m) and the reduced quantum efficiency of the mesh PM's, halving the number of photoelectrons.

In sum, we have studied extensively the performance of both the *barrel* and *end-cap* prototypes of the KLOE calorimeter and confirmed the findings with module IHEP. Aside from the measured energy and time resolutions quoted, we found the energy resolution to be independent of the incidence angle and we expect very little dependence of the time resolution on incidence. We have verified that the calorimeter can provide some added means to identify pions and muons. Finally, the KLOE electronics performed extremely well at the PSI test, fully to specifications and with very low noise. Therefore, we have succeeded in the design of a calorimeter which satisfy, with some safety margins, the requirements of the KLOE experiment.

## 5. 2 Calorimeter performance

Table 4. Calorimeter Performance.

$\delta(\text{Shower Apex}) = 1\text{ cm}$
$\delta E/E = 5\%/\sqrt{E\text{ (GeV)}}$
$\delta t = 60\text{ ps}/\sqrt{E\text{ (GeV)}}$

## 6 – Magnet

Of crucial importance in rejecting contamination of the  $K_L \rightarrow \pi^+ \pi^-$  sample is the ability of performing good measurements of momenta in the range 155–268 MeV/c. In particular  $K_{\mu 3}$  decays overlap kinematically  $K_L \rightarrow \pi^+ \pi^-$  decays when the laboratory muon momentum is  $\sim 250\text{ MeV}$ . A simple argument predicts that kinematical overlaps decrease as the cube of the field value. This has been proved by full Monte Carlo calculations. A possible argument against high field is the loss of tracking efficiency and accuracy in vertexing for spiraling tracks. Again we barely see a loss in tracking efficiency beginning at 7 kG,  $\sim 0.2\%$  as well as some saturation in the  $K_{\mu 3}$  background rejection. This justifies our choice of 6 kG, which provides good rejection without impairing other detector functions. The chamber and calorimeter are inside a superconducting coil and the iron return yoke has deep cavities hollowed out so that the magnetic field therein is reduced and axial, to allow the proper functioning of the mesh photomultipliers employed in the EmC readout. Economical reasons, *i.e.*, power consumption, made us choose a superconducting coil.

## 7 – Front-end Electronics

The KLOE detector contains 5,000 photomultipliers, PMs, for the readout of the calorimeter, and  $\sim 13,000$  wires for the tracking chamber. The PM signals are amplified in the PMs' bases and sent to analog boards of 30 channels each. The outputs of this board are connected to ADCs, TDCs and to the

trigger processor. The chamber signals are preamplified at the wire feed-through and sent to boards of 48 channels each. The output of two of these boards are connected to a 96 channel TDC board for drift time measurements.

Module IHEP tested to great satisfaction the following chain of the final KLOE electronics at PSI in June 1994: PM bases containing the voltage divider and an A.C. coupled preamp which drives the cables carrying the signals to the outside, splitters which provide input to a constant fraction discriminator and to a driver for amplitude measurements, the KLOE designed 12 bit ADC's and 12 bit TDC's.

The TDC chips for the KLOE chamber digitization will reside in groups of three (96 channels) on modules fitting into the KLOE custom crates and readout scheme. Most of the functionality, digitization and event buffering, is integrated into a VLSI chip. The measurement of the signal drift-time coming from the chamber is performed by a custom integrated circuit, which is developed by the INFN Sezione di Roma1. The circuit is a multichannel common start/stop TDC, with 32 channels per chip. In KLOE the drift-time measurement is done by recording, for each signal, its time of arrival with respect to a stop signal, which is common to all channels and generated by the trigger. The TDC integrated circuit is developed as a full-custom device in 0.5 micron CMOS technology. Its working frequency is a function of an external reference clock that must be supplied to the circuit and it can be as high as 1 GHz (1 nsec LSB). The circuit is capable of detecting rising/falling edges, with a double edge resolution of 10 nsec or better. A programmable number of hits, from 1 to 16, can be stored for each channel. The hits are recorded as 16 bit words and every registered hit is stored in the chip for a programmable time interval. If during this time the chip does not receive a stop command the hit is removed, otherwise, the hit is kept for the read-out. The chip has also a multi-event buffering capability, 4 events deep, which is used only if at least one hit is present in one of the 32 channels, in a time window associated with a stop signal. Dedicated prompt trigger output lines inform the read-out of the presence in the chip of data to be read. The read-out of the data passes through the I/O port at a maximum speed of 50 MHz. The empty channels are automatically skipped during the read-out phase and for each registered hit the chip gives its absolute time value with respect to the stop signal and its channel number. Additional chip functions include an event counter, masking of the individual channels, and a self-test facility.

## 8 - Data Acquisition

$\phi$  decays and calibration events represent, at full DAΦNE luminosity, a very large load for the data acquisition system. At 10,000 events per second, each event consisting of 2 to 4 kBytes, we estimate that 20,000 MIPS equivalent computing power will be necessary to digest the data. The universal approach appears to be farms of the new powerful  $\mu$ -processors. We are looking at the  $\alpha$ -VAX product of DEC, capable of 120 MIPS, amongst possible choices. We intend to write to tape all raw data, and we need to perform Monte Carlo simulations at the  $10^8$ , or greater, event level. The data produced in one year at full  $\mathcal{L}$  is  $\sim 4 \times 10^{14}$  Bytes, to be stored at a bandwidth of 50-100 MBytes/s. The new Digital Linear Tapes, DLT by DEC, seems capable of such task. Due to the Monte Carlo simulation needs and the inevitable necessity of running production more than once we plan on two 20,000 MIPS farms. The major components of the KLOE DAQ system are briefly presented in the following.<sup>[15]</sup> Data comes from  $\sim 25,000$  Front End Electronics channels housed in some 40 9U-VME crates. Signal conditioning and digitization is performed in a fixed time of  $\mathcal{O}(2 \mu s)$ , to avoid biases depending on event configuration. Every FEE channel contains buffers of appropriate depth, in order to eliminate data overflows and to allow

asynchronous read-out. Data from the FEE are transferred to an on-line farm of Single Board Computers, SBC, using a two level concentration scheme. The first one is performed at crate level via a custom bus in the backplane, the AUXbus, and a hardwired read-out controller, ROCK, located in the crate itself. The ROCK implements the function of a sparse readout scanner collecting data related to each single trigger. The second level of concentration is performed by a ROCK manager, ROCKM, connected to chains of crates of suitable length with a cable bus, Cbus. Each ROCKM resides in a 6U-VME crate together with a VME processor which prepares sub-events for transmission to a given farm element. A commercial VME interconnector, VIC, connects all the crates in a chain allowing VME processors to program, check and debug FEE, ROCK's etc. The components of the DAQ system are interconnected via Ethernet for low bandwidth operations (controls, downloading, monitoring) and via FDDI for data transmission. A DEC FDDI GIGAswitch, with bridge functionality, is used to provide parallel paths between the VME processors and the farm in a scalable way. The number of switch ports dedicated to chains is chosen taking into account two factors: the maximum acceptable read-out ROCKM time and the throughput of the communication protocol achievable at VME and farm level. In order to improve the performance of the communication protocol, the sub-events related to the same group of consecutive trigger numbers are packed in sub-event-strings that must be gathered by a single SBC. The farm SBC's build and test the integrity of each event, implement the final event formatting, and perform quality control on samples of the data. The address of each farm element is assigned by an additional VME processor, the data flow controller, DFC, connected also via VIC channels to the ROCKM crates. The DFC manages the load of all the VME processors, maintaining a table which maps groups of trigger numbers and SBC addresses. DAQ resets and buffer flush-out commands are generated when misalignment is detected at farm level. Other error conditions will be similarly handled. The farm is based on SBC's organized in crates. Each crate has a dedicated output SBC which manages the crate I/O to the storage devices. The total CPU power required for the whole farm is estimated to be about 16,000 Specint'92. CPU boards adequate for this are beginning to appear in the market. We wait for a final decision upon the outcome of a joint project between INFN and DEC designing a custom SBC using the DEC Alpha chip.

### **Acknowledgments**

I wish to thank the Corfu School organizers for their kind hospitalities. Also, I wish to acknowledge and thank all my KLOE colleagues for their brilliant, wonderful and heroic efforts to realize KLOE. I also wish to thank Paula J. Franzini for help in preparing this paper.

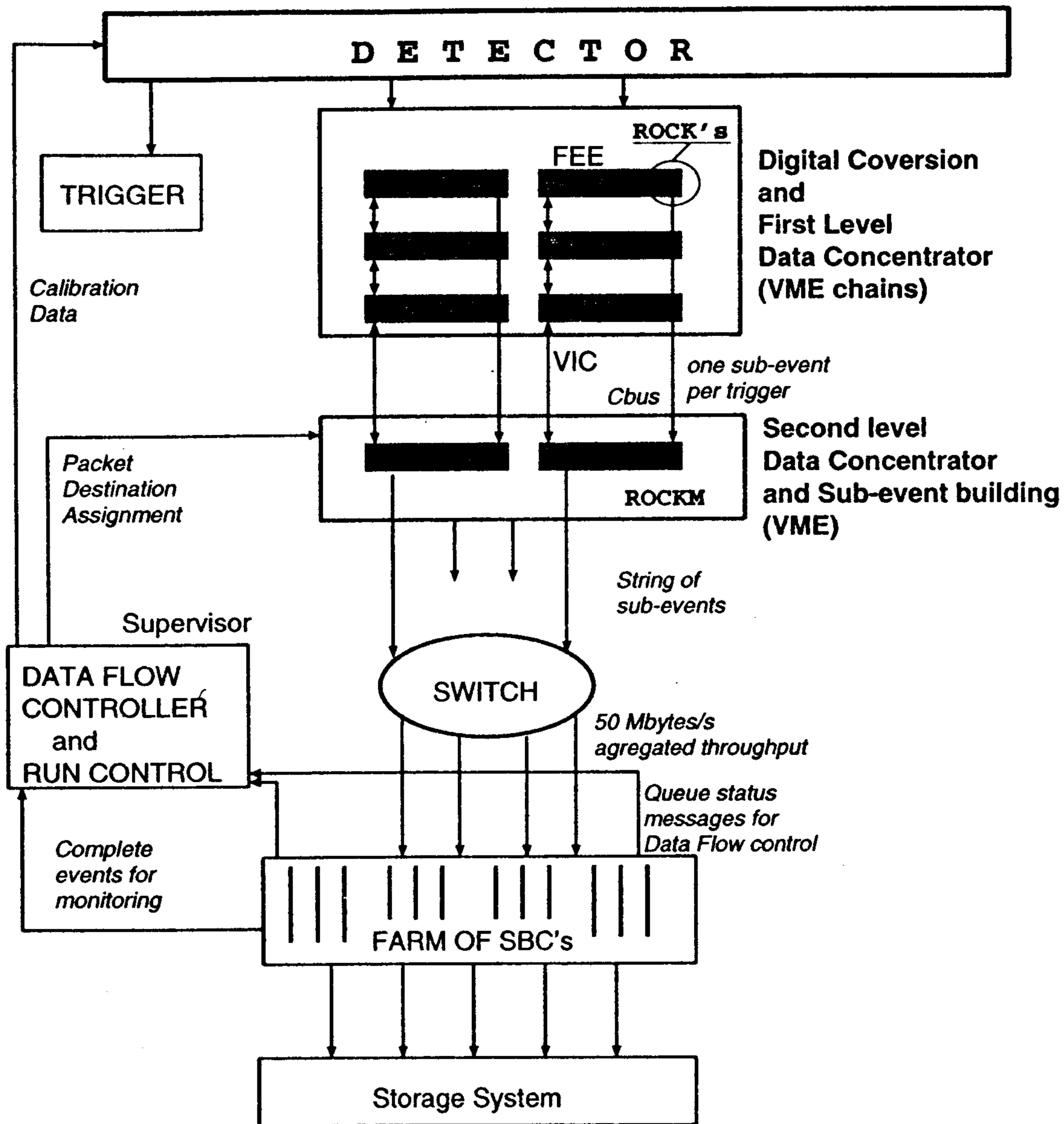


Fig. 15. System Architecture and Information Flow.

## REFERENCES

1. C. D. Buchanan *et al.*, Phys. Rev. **D45**, 4088 (1992).
2. L. Maiani, *The DAΦNE Physics Handbook*, L. Maiani *et al.* Eds., Frascati, 1992, p. 21.
3. For all references on CHPT, see *The DAΦNE Physics Handbook*, ed. L. Maiani *et al.*, LNF, Frascati.
4. M. Baillargeon and P. J. Franzini, *The Second DAΦNE Physics Handbook*, eds L. Maiani, G. Panzeri and N. Paver, LNF Frascati, 1995, p. 413.
5. F. E. Close, *The DAΦNE Physics Handbook*, p. 465, 1992.
6. J. Lee-Franzini, W. Kim, and P. J. Franzini, *The DAΦNE Physics Handbook*, p. 533.
7. J. Lee-Franzini, W. Kim, and P. J. Franzini, Phys. Lett. **B287** 259 (1992); *The DAΦNE Physics Handbook*, p. 513.
8. A. Bramon, G. Colangelo, P. J. Franzini and M. Greco, *The DAΦNE Physics Handbook*, p. 487.
9. P. J. Franzini and G. Colangelo, Phys. Lett. **B289**, 189 (1992).
10. T. Kinoshita, B. Nizic and Y. Okamoto, Phys. Rev. D **31**, 2108 (1985), and references therein; see in particular their reference 28.
11. P. Franzini, *The Second DAΦNE Physics Handbook*, eds L. Maiani, G. Panzeri and N. Paver, LNF Frascati, 1995, p. 471.
12. *KLOE, A General Purpose Detector for DAΦNE*, the KLOE Collaboration, LNF Report LNF-92/019, April 1992.
13. "THE KLOE DETECTOR, *Technical Proposal*." the KLOE Collaboration, LNF-93/002 (IR), January 1993.
14. *The KLOE Central Drift Chamber*, the KLOE Collaboration, LNF Report LNF-94/028, 1994.
15. *The KLOE Data Acquisition System*, the KLOE Collaboration, LNF Report LNF-95/014, 1995.
16. J. H. Christenson *et al.*, Phys. Rev. Lett. **13**, 138 (1964).
17. A. Antonelli, C. Bloise and A. Calcaterra, KLOE Notes 3, 23.
18. F. Grancagnolo, with the KLOE Chamber Group, Vienna Wire Chamber Conference 1995.
19. G. de Zorzi, *Proc. of 4th Int. Conf. on Calorimetry*, eds. A. Menzione and A. Scribano, World Scientific, 1993 P. 187.
20. A. Di Domenico *et al.*, KLOE Notes 83 and 84.
21. C. Bini *et al.*, KLOE Notes 42, 50, 60, and 78; G. Barbiellini *et al.*, KLOE Notes 56 and 81.
22. F. Bossi, KLOE Notes 54 and 91.
23. L. Keeble, G. Lanfranchi and M. Anelli, KLOE Notes 90, 96 and 109.